RESEARCH ARTICLE

Basin Research   IAS EAGE   WILEY

A regional CO_2 containment assessment of the northern Utsira Formation seal and overburden, northern North Sea

Christopher Lloyd[1] (iD) | Mads Huuse[1] (iD) | Bonita J. Barrett[2] (iD) | Margaret A. Stewart[3] | Andrew M. W. Newton[4] (iD)

[1]Department of Earth and Environmental Sciences, University of Manchester, Manchester, UK

[2]Equinor ASA, Equinor Research Centre, Ranheim, Norway

[3]British Geological Survey, Edinburgh, UK

[4]School of Natural and Built Environment, Queen's University Belfast, Belfast, UK

Correspondence
Christopher Lloyd, Department of Earth and Environmental Sciences, University of Manchester, Manchester, UK.
Email: Christopher.lloyd-2@manchester.ac.uk

Funding information
Natural Environment Research Council

Abstract

Upscaling Carbon Capture and Storage requires identification of suitable storage sites, with robust reservoir seals. The Utsira Formation in the northern North Sea has been flagged as a target for further storage. However, there are no regional studies of seal variability addressing heterogeneities that could facilitate seal bypass. This study aims to: (a) identify, assess and map the elements that promote or restrict fluid migration, (b) develop a matrix to regionally map containment confidence (CC) and (c) rank the different areas for CO_2 containment across the Utsira Formation. The seal and overburden were mapped using a high-resolution, pre-stack depth-migrated 3D broadband seismic reflection dataset and 141 exploration wells. Seal geometry, sandstone presence and sandstone connectivity in the seal and overburden were assigned relative CC scores, which were summed to map overall CC of the Utsira Fm. Indicators for shallow gas and migration were mapped and correlated with the other elements. Areas with the lowest CC are in the west of the Utsira Fm. Here, sandstones within the Seal Interval are connected through the overburden via sandy submarine fans. In the southeast, dipping stratigraphy downlaps onto the Utsira Fm., increasing the potential for connection with glacially-derived channel-lobe systems in the overburden. The areas with the highest CC are the central and northeast parts of the Utsira Fm., where the Seal Interval is mudstone-dominated and parallel to the reservoir, and channel-lobe systems identified in the Overburden Interval are disconnected from the reservoir. This area coincides with a thick depocentre of the northern Utsira Fm. These results can be used to inform CO_2 storage site selection and constrain future CO_2 plume simulation analyses for the Utsira Fm. The CC matrix outlined here can also be adapted and applied to regionally assess the containment of other potential CO_2 storage reservoirs in any setting.

KEYWORDS

containment confidence, CO_2 containment, CO_2 storage, clinoforms, CCS, geomorphology, migration risk, seismic analysis, Utsira Formation

1 | INTRODUCTION

Large-scale Carbon Capture and Storage (CCS) projects will be critical for developing the low carbon solutions required to reduce net CO_2 emissions (IEA, 2016, 2017; Stocker, 2014). There are currently 26 operational large-scale CCS facilities globally, with a combined capture capacity of ca. 40 Mt CO_2/yr (GCCSI, 2020; Ringrose & Meckle, 2019). However, by 2050, European CO_2 storage demand is expected to reach up to 300 Mt per year (European Commission, 2018). Thus, upscaling of CCS is a critical challenge, particularly identifying suitable storage sites, where reservoir seals must be capable of retaining 99% of the CO_2 after 100 years post-injection (Chadwick et al., 2008; Hepple & Benson, 2005).

The North Sea subsurface contains over two thirds of the CO_2 storage capacity of northwest Europe (Höller & Viebahn, 2011). It is a prolific hydrocarbon region, proving that fluid can be stored in its formations for millions of years. Combining ca. 50 years of subsurface expertise, the availability of existing infrastructure and the proximity to market means the North Sea has excellent potential to be a European hub for CO_2 storage. The southern region of the Utsira Formation (Fm.) contains the Sleipner CO_2 injection site, which has been operational since 1996 and is one of only four dedicated CO_2 storage projects injecting into saline aquifers (Chadwick et al., 2004; Ringrose & Meckle, 2019) (Figure 1a). The Utsira Fm. has been highlighted as a potential target for further storage due to its large size (ca. 29,300 km^2 from NPD FactMap, 2019) and good reservoir properties (ca. 35% average porosity, >1 D permeability at Sleipner) (Lie et al., 2016; Singh et al., 2010; Zweigel et al., 2004). The northern part of the formation is understudied relative to its southern counterpart due to its shallower burial depth and reduced thickness. However, it could be a prospective area for upscaling of CCS. CO_2 storage studies on the Utsira Fm. have generally focused on the storage capacity for either the full formation (Gasda et al., 2017; Halland et al., 2011; Thibeau & Mucha, 2011), for discrete structural traps (Chadwick et al., 2008) or both (Bøe et al., 2002; Holloway, 1996; Thibeau et al., 2018). These studies either assume complete seal integrity or inject CO_2 until the maximum sealing pressure capacity is reached (Gasda et al., 2017; Thibeau & Mucha, 2011). The transition from theoretical storage to actual storage requires confidence that the CO_2 will remain in the reservoir. However, no studies have addressed regional heterogeneities within the seal that could facilitate localised seal bypass, nor have they presented a regional assessment of seal variability. Understanding the seal variability and its effect on containment is crucial for CO_2 storage site selection and is the focus of this study. Moreover, having a robust regional understanding of the seal is important for risk assessment and mitigation, as reservoir fluid could migrate within the reservoir to less favourable sealing areas.

Highlights

- There is not a laterally-extensive and homogenous seal above the Utsira Formation.
- Regional high-resolution data and modern interpretation approaches illuminate potential seal bypass systems.
- A novel containment confidence matrix is used to rank the potential CO_2 storage areas.
- The workflow for detailed seal and overburden assessment is highly applicable to other basins.

This study addresses the containment challenge using regional 3D seismic reflection data correlated with petrophysical and geological data from 141 exploration wells to investigate the stratigraphy above the northern Utsira Fm. This work: (a) identifies, assesses and maps seal and overburden elements that promote or restrict fluid migration from the Utsira Fm; (b) develops a matrix integrating these elements to regionally map containment confidence (CC), with consideration of uncertainties and (c) identifies the best and worst regions for containment of CO_2 and discusses the implications for upscaled CO_2 storage in the northern North Sea.

2 | GEOLOGICAL SETTING

The northern North Sea experienced two separate episodes of major lithospheric stretching in the Mesozoic (Coward et al., 2003; Færseth, 1996; Nøttvedt et al., 1995). Initially, east–west to eastnortheast–westsouthwest-oriented extension occurred in the late Permian, resulting in the formation of a 130–150 km wide, north–south-orientated basin. A second phase commenced in the Middle Jurassic, where northwest–southeast-orientated extension led to generation of new Jurassic faults and reactivation of older Permo-Triassic faults (Coward et al., 2003; Færseth, 1996). As well as the North Viking Graben (NVG), these episodes produced a series of structural elements in the northern North Sea, including: (a) the East Shetland Platform (ESP), a regional platform to the west of the NVG that prevailed as a high through the Cenozoic (Platt & Cartwright, 1998); (b) the Horda Platform, a regional platform to the east of the NVG and (c) the Tampen Spur, a series of rotated fault blocks to the northwest of the NVG and north of the ESP (Figure 1b,c). Subsequent deposition was highly influenced by the antecedent structural relief created by rifting and post-rift thermal subsidence (Bugge et al., 2001).
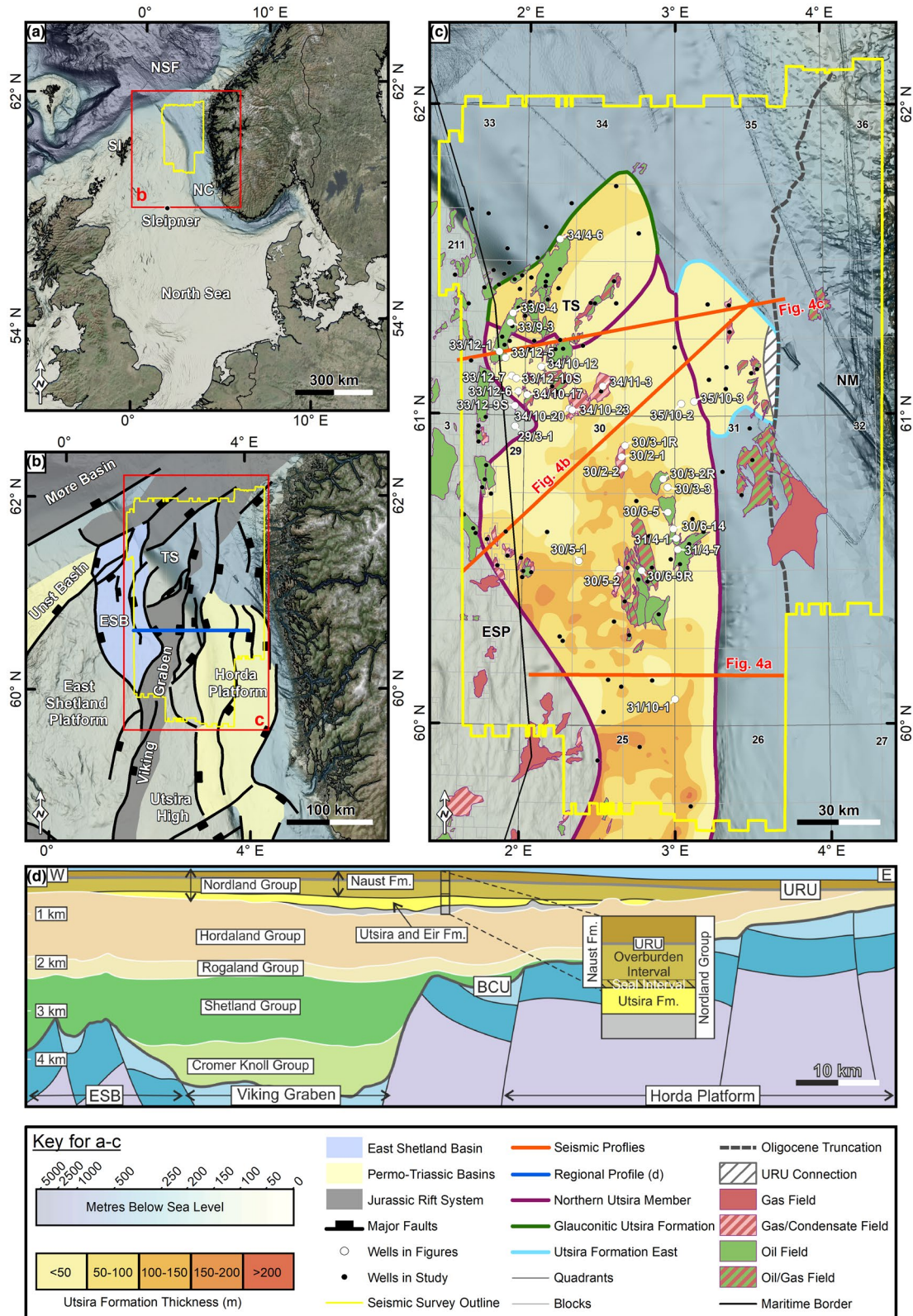
FIGURE 1 Study area with wells and data extent. (a) Context of the study area in the North Sea and the location of the Sleipner injection site. Satellite imagery from the World Imagery layer of ArcMap online. Bathymetry from EMODnet Bathymetry Consortium (2018). (b) A simplified map showing the main structural elements in the study area (modified from Færseth et al., 1996). (c) Utsira Fm. thickness map (Eidvin et al., 2013) with seismic dataset extent (yellow box). Dots show wells used in this study, and data from those highlighted in white are presented in this study. Oil and gas fields in the region are also indicated. (d) Regional west-east profile of the Jurassic Rift and overlying stratigraphy split into groups to show main structural elements for reference. Inset shows the studied interval. ESP, East Shetland Platform; NC, Norwegian Channel; NM, Norwegian Margin; NSF, North Sea Fan; SI, Shetland Islands; TS, Tampen Spur region

The Cenozoic was characterised by exhumation of the North Sea basin margins and surrounding landmasses, resulting in up to 2,500 m of sediment being deposited in the subsiding basin (Jordt et al., 1995; Martinsen et al., 1999), comprising the Rogaland, Hordaland and Nordland Groups (Isaksen & Tonstad, 1989) (Figure 1d). The upper section of the Hordaland Group contains the Skade Fm. close to the ESP, with mudstones in the distal part of the basin, which were later polygonally faulted (Rundberg & Eidvin, 2005; Wrona et al., 2017). The Hordaland and Nordland Groups are separated by the Top Hordaland Group Unconformity (THGU), reflecting a phase of plate tectonic reorganisation and associated uplift of the North Sea basin margins and fall in relative sea level (Eidvin et al., 2013; Galloway, 2002; Løseth et al., 2013; Martinsen et al., 1999; Rundberg & Eidvin, 2005).

The Eir Fm. is the first Nordland Group formation deposited above the THGU in the northern North Sea, comprising sandstones with minor mudstones above the NVG, with time-equivalent mudstones deposited above the South Viking Graben (Eidvin et al., 2013, 2014). The Eir Fm. is overlain by the Utsira Fm., which is preserved as a north–south trending, >450 km, elongated, mature sandstone with minor mudstones (Eidvin et al., 2013; Rundberg & Eidvin, 2005) (Figure 1c). Both the Eir and Utsira Fm. were mainly sourced from the ESP, through deposition into an epeiric shelf sea, connecting the southern North Sea to the Møre Basin (Eidvin et al., 2013; Galloway, 2002; Gregersen & Johannessen, 2007; Isaksen & Tonsetad, 1989; Rundberg & Eidvin, 2005). To the north, the Utsira Fm. has been subdivided into higher-order units, which are differentiated based on composition (Glauconitic Utsira Formation) or provenance (Utsira Formation East) (De Schepper & Mangerud, 2017; Eidvin et al., 2013; Løseth et al., 2020) (Figure 1c).

The overlying sediments that comprise the seal and overburden of the Utsira Fm. are termed the Naust Formation in the Norwegian Sea (Dalland et al., 1988), and this nomenclature has been extended into the North Sea stratigraphy (Batchelor et al., 2017; Eidvin et al., 2013; Løseth et al., 2020; Ottesen et al., 2014, 2018). In the northern North Sea, the Naust Fm. represents up to 1,000 m of sediments in the basin centre (Eidvin et al., 2013; Ottesen et al., 2012, 2014). It has been subdivided into four stratigraphic intervals (A, B, C and D), which are intervened by the Upper Regional Unconformity (URU); a diachronous feature that is present over much of the North Sea, and is related to significant glacial influence and erosion of the Norwegian Channel (Batchelor et al., 2017; Løseth et al., 2020; Ottesen et al., 2014, 2018). Beneath the URU, the Naust Fm. units are characterised by prograding clinoforms from the eastern (Norwegian Margin (NM)) and western (ESP) sides of the basin. The western clinoforms are fed from a fluvio-deltaic system on the ESP, which transported sands into the basin mainly through turbidity currents. The eastern clinoforms have a predominantly glaciofluvial and subglacial origin and contain glaciogenic debrites, formed from remobilisation of subglacially derived sediment (Batchelor et al., 2017; Eidvin et al., 2013; Løseth et al., 2020; Ottesen et al., 2014). In the northern study area, this interval may also contain sandstone extrudites from deeper sourced remobilised sediment (Løseth et al., 2012, 2013). This pre-URU Naust Fm. interval has reduced thickness at 60°N, where accommodation is restricted, but at ca. 61°N (in a distal position from the ESP), the basin widens and deepens and the west-dipping NM clinoforms dominate the stratigraphy (Løseth et al., 2020; Ottesen et al., 2014). In the east, where the URU eroded more deeply, most of the NM clinoform topsets are truncated.

Above the URU, the Naust Fm. is dominated by deposition from the west, and was largely influenced by Quaternary glaciations in terms of deposition and reworking (Ottesen et al., 2014; Stewart et al., 2013). Glacial features observed in this interval include iceberg ploughmarks, mega-scale glacial lineations, glaciogenic debrites and occasional tunnel valleys (Ottesen et al., 2020). North of the Utsira Fm. extent, there is a large feature, previously described as the early Pliocene Canyon (Eidvin & Rundberg, 2001) or Sunnfjord Channel (Løseth et al., 2020).

3 | STUDY AREA AND DATASET

This study focuses upon the lower interval of the Naust Fm. (stratigraphy below the URU), directly overlying the northern part of the Utsira Fm., from 30 km south of 60°N to 62°N (Figure 1). The geographic boundaries of the study are defined by the extent of the 35,400 km² 3D BroadSeis™ seismic reflection survey of the North Viking Graben (NVG), acquired and provided by CGG. The survey reaches 9 s two-way travel time (TWT) and images Mesozoic structural features either side of the NVG: the ESP and Tampen Spur (TS) on the western side and the Horda Platform (HP) on the eastern side (Figure 1b). These features are used as spatial reference points in this study. The original seismic TWT data were converted into depth by CGG, using advanced full-waveform inversion, to iteratively estimate the subsurface velocity field, which included absorption effects caused by shallow features (Hayes et al., 2018). The depth converted data were cross-checked with well data and appeared to tie well. The dominant wavelength of the seismic reflection depth data in the interval of interest was measured as ca. 20 m, providing a vertical resolution of ca. 5 m ($\lambda/4$) and limit of detectability of ca. 0.7 m ($\lambda/30$). The sub-sampled line spacing is 37.5 m in the in- and cross-line directions, which is greater than the migrated Fresnel zone and thus is the main limitation in horizontal resolution. Seismic data are presented as zero phase and with the American polarity convention, whereby a

downwards increase in acoustic impedance is represented by a positive reflection and the peak is shaded with blue.

Petrophysical and geological data from 141 exploration wells from the UK and Norway were used in this study. The wells are generally clustered, as they targeted prolific hydrocarbon provinces (Figure 1c). This, combined with the shallow depth of the studied stratigraphic interval (<1,200 m TVD) (Figure 1d), means the spatial distribution and quality of relevant well data are highly variable. Wells were selected with a two-fold criteria: (a) the well should penetrate the Utsira Fm. or Naust Fm. clinothems that connect to the Utsira Fm.; and (b) there is an accompanying interpreted lithological column, provided by Tomlinson Geophysical Services Inc. (TGS) through their Facies Map Browser (FMB) tool. The TGS FMB tool is a global database (with a sub-database for the North Sea) containing the raw log data with TGS interpretations for open-access wells. The FMB lithological column was generated using petrophysical logs (e.g. gamma, resistivity, neutron, density) and well completion reports. Logs are not always recorded in the shallower stratigraphy, and therefore only a subset of the exploration wells had this lithology interpretation in the studied interval. Eighteen wells that were missing the FMB lithology column were included in the analysis to improve spatial distribution. These wells typically had either missing or poorer log data. Lithologies in these wells were manually interpreted from gamma ray logs and well completion reports, where available and of sufficient quality.

4 | METHODOLOGY

To characterise the overburden, each element that could be responsible for potential fluid migration upon CO_2 injection into the Utsira Fm. was assessed, following the workflow in Figure 2a. Two stages of data preparation were undertaken: (a) normalisation of the well lithologies and nomenclature into broad, simplified groups (Figure 3); and (b) definition of a seismic stratigraphic framework (Figure 4). To focus on sandstone versus mudstone lithologies and to allow easier correlation between wells, the interpreted lithologies from FMB have been broadly grouped into 'sandstone', 'mudstone' and 'other' lithologies. Simplified lithologies 'sandstone' and 'mudstone' account for 14.5% and 85.3% of the studied interval respectively (Figure 3).

To stratigraphically constrain sandstone deposits, a seismic framework was established in which the studied interval (top Utsira Fm. up to the URU) was divided into six units, which represent the depositional evolution of the basin (Figure 4). Previous studies take a similar approach by splitting the stratigraphy into four (Batchelor et al., 2017; Løseth et al., 2020; Ottesen et al., 2014, 2018) or three (Gregersen & Johannessen, 2001, 2007) seismic stratigraphic units. Units

were defined through manual interpretation of the seismic reflection data considering stratal geometries, amplitudes and thickness patterns that highlight the main bounding surfaces, using a combination of 2D and 3D auto-tracking tools (Petrel™ software). The unit boundaries were selected for three reasons: (a) to follow closely with the unit divisions of previous work (Ottesen et al., 2014, 2018); (b) to further subdivide the immediate stratigraphy overlying the reservoir for the seal assessment and (c) to adhere to the most regionally consistent and strongest reflections. Intra-unit surfaces (in chronological order Top Unit 1, 2.1, 2.2… Top Unit 2, etc.) were generated using semi-automated horizon generation and were assessed using cross-section validation. This approach for semi-automated horizon generation in Paleoscan™ is summarised by Daynac et al. (2016). The manually interpreted unit boundaries provided geological constraints for the semi-automated horizons, which were iteratively checked for geological accuracy.

The seal and overburden were assigned separate intervals to differentiate the stratigraphy responsible for containing CO_2 in the reservoir ('Seal Interval') from the overlying stratigraphy ('Overburden Interval') (Figure 2b). Here, the Seal Interval is defined as the minimum thickness of mudstone required for sealing, which depends upon its sealing integrity in any given case. Without access to data on this, a Seal Interval of 50 m is used here, which is the advised minimum thickness of a seal for CO_2 storage in the North Sea (Halland et al., 2011). The Seal Interval does not correspond to a seismic stratigraphic unit (as defined above), rather represents a 50 m 'buffer' directly above the Utsira Fm. The overlying succession up to the URU is the 'Overburden Interval'. Seal geometry, sandstone presence and sandstone connectivity were analysed to identify heterogeneities and potential migration paths (CO_2 Containment Analysis in Figure 2a). Potential shallow gas and gas migration indicators were highlighted to support the analysis, as evidence of trapped fluid and fluid flow.

4.1 | Seal geometry assessment

Flat-lying stratigraphy provides a better reservoir seal than dipping stratigraphy for two reasons. Firstly, dipping stratigraphy (e.g. clinoform foresets) juxtapose more sub-units against the reservoir, increasing the risk of a high-permeability zone (sandstone) being in contact with the reservoir. Secondly, an entire succession of sandy clinothems would be required for vertical migration in flat-lying stratigraphy, whereas a sandy bed within a single clinothem is required for vertical migration in dipping stratigraphy (Figure 2b). The spatial variability in seal geometry was assessed by creating a pseudo-surface, parallel to and 50 m above the Top Utsira Fm. surface (to define the top of the 'Seal Interval'). Seismic
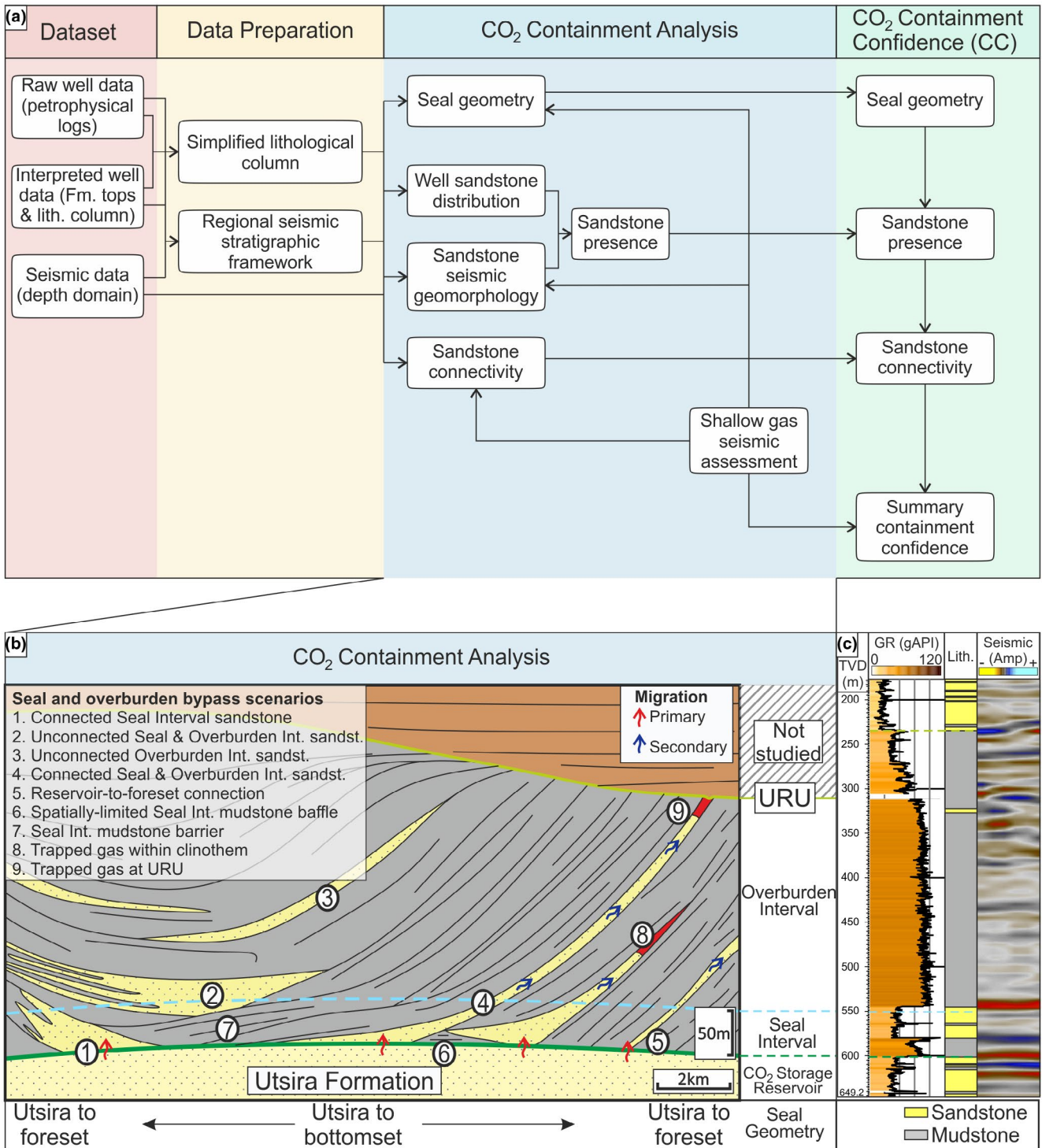
FIGURE 2 Workflow and seal bypass concepts. (a) The full workflow followed in this study, utilising three datasets. (b) Schematic cross-section of the seal and overburden bypass scenarios through primary and secondary migration. 'Primary migration' refers to migration from the reservoir to the Seal Interval. 'Secondary migration' refers migration from the Seal Interval to and through the Overburden Interval. Trapped shallow gas in the overburden (8) or at the URU (9) can support the interpretation of fluid migration pathways. (c) Seismic well tie for well NO 30/5-2 showing the seismic response for a sandstone and mudstone boundary. The sandstone within the Seal Interval extends 5 m into the Overburden Interval. Amp., amplitude; int., interval; Lith., lithology; sandst., sandstone; URU, Upper Regional Unconformity

amplitudes were assessed at this level to show the geometry of the clinoforms in plan view, by either revealing alternating positive–negative amplitude bands where the surface slices dipping clinoform foresets, or broad areas of a single polarity where the surface slices flat-lying or parallel-to-reservoir, clinoform bottomsets.
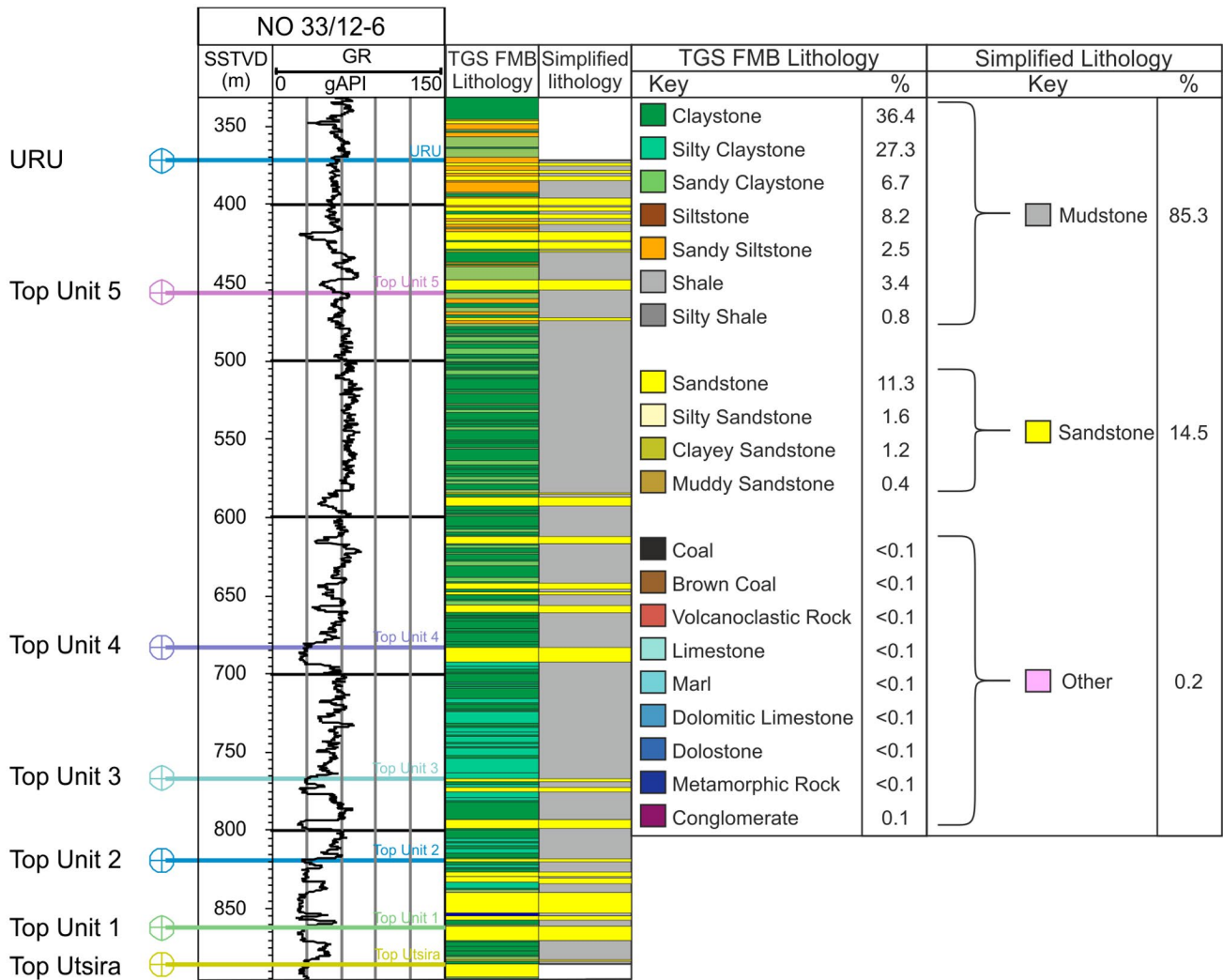
FIGURE 3 FMB lithology column with simplification used for this study. The studied interval is from the top Utsira Fm. to the Upper Regional Unconformity (URU). TGS FMB lithology percentage (%) refers to the total percentage of each lithology that is present within the studied interval in the 123 wells that had FMB interpreted lithology columns. Simplified lithology percentage (%) refers to the total percentage of each simplified lithology for the same interval and wells. Most of the studied interval comprises 'mudstone' (85.3%)

4.2 | Identification of sandstones

Sandstones that are proximal to the reservoir provide the greatest risk to containment of CO_2 (Figure 2b). In the studied interval, sandstones have a lower acoustic impedance than the mudstones, and therefore the top of a sandstone bed (mudstone to sandstone transition) is represented by a soft response (red) and the base (sandstone to mudstone transition) is represented by a hard response (blue) (Figure 2c). Using seismic unit thickness maps and the sandstone percentages in the well data for each of the six units, regions of high sandstone content were identified.

In addition, the following seismic attributes were used to interpret sandstones: (a) sweetness, which reduces the contribution of high-frequency events, where high amplitudes and low frequencies (i.e. sandstone) will have high sweetness; (b)

variance, an amplitude invariant measurement of trace-to-trace continuity, useful for detecting channel/lobe features on surfaces and (c) spectral (frequency) decomposition, which highlights the individual frequencies of a wavelet thereby improving thin bed resolution and showing bed thickness variability. Variance and spectral decomposition were used in conjunction to highlight seismic geomorphologies, that is, variance highlights the edges of a channel or lobe, and spectral decomposition highlights the channel thickness variability (Section 5.4). Spectral decomposition was performed using frequencies of 17 (red), 24 (blue) and 38 (green) cycles per km (c/km) to cover the frequency spectrum (GeoTeric™ software). Every high-amplitude clinoform was analysed to identify potential sandy features that could act as up-dip fluid migration pathways (Figure 2b).

The presence and lateral extent of all of the seismically resolvable sandstone bodies are characterised based on a
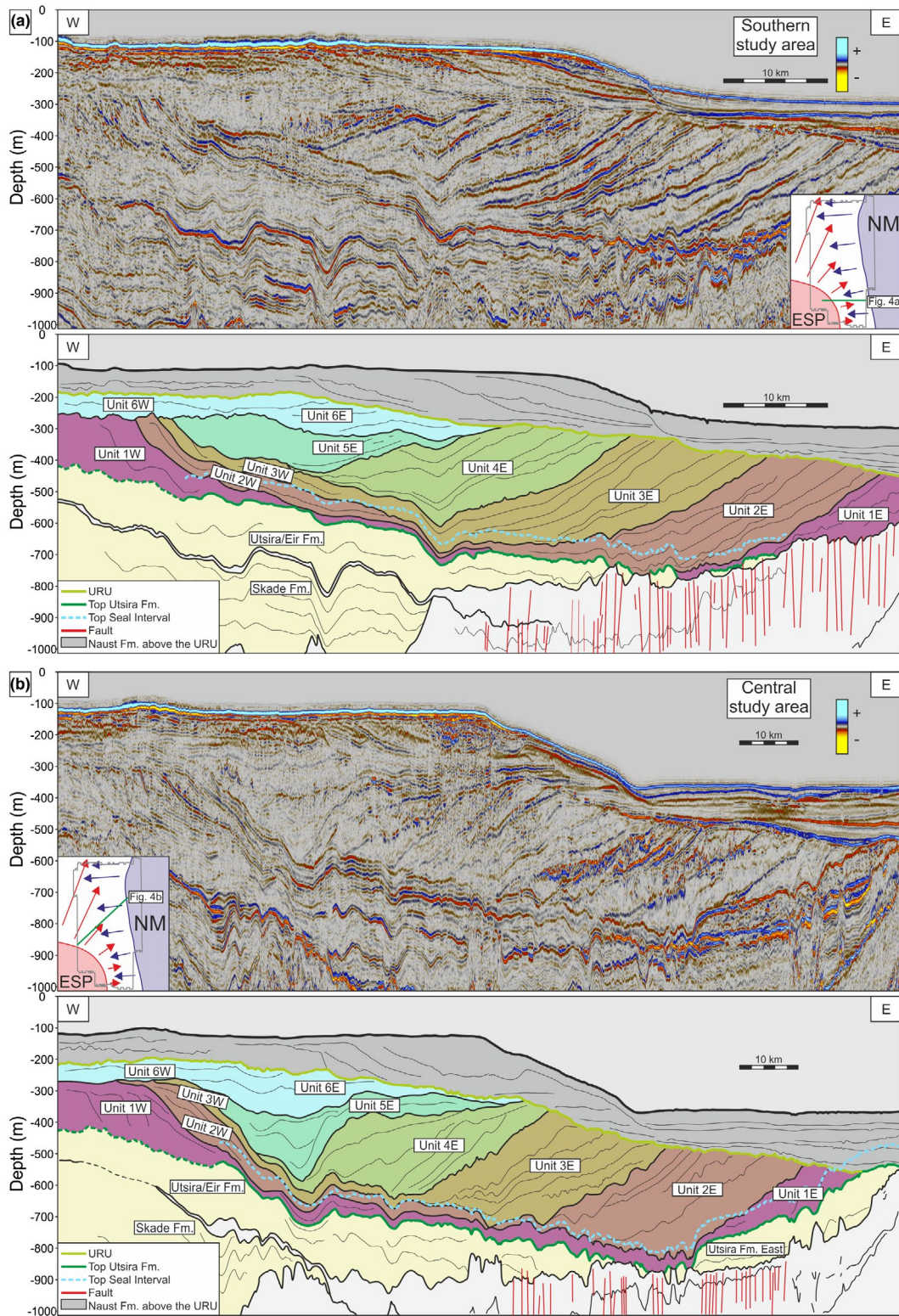
FIGURE 4 Seismic cross-sections and interpretations for the stratigraphic sub-divisions of the Utsira Fm. seal and overburden. Cross-sections extend across the southern (a), central (b) and northern (c) regions of the study area. Lines trend from the East Shetland Platform (ESP) in the west to the Norwegian Margin (NM) in the east. The stratigraphic interval of interest is from the Top Utsira Fm. to the Upper Regional Unconformity (URU). Positions of cross-sections shown in Figures 1 and 6 and in insets. Insets also show the main progradation direction (arrows) of the ESP (red) and NM (blue) shelves
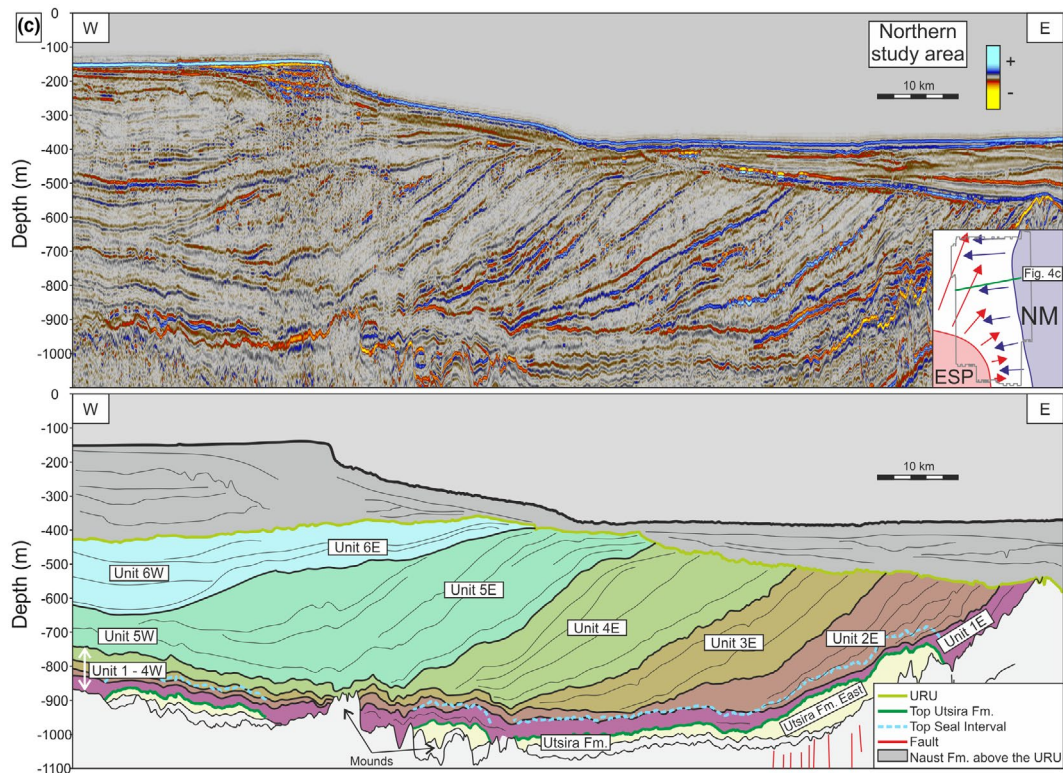
FIGURE 4   (Continued)

three-tier classification: (a) 'proven' sandstones that can be correlated between wells and on seismic; (b) 'probable' sandstones based on extrapolation of proven sandstone bodies beyond the wells containing the sandstone, limited by a change in seismic expression or when encountering a correlatable mudstone in a neighbouring well and (c) 'possible' sandstones that are not penetrated by any wells but have either a seismic response similar to that of a nearby proven sandstone, or a geological feature identified from the seismic geomorphology analysis (Table 1). This gave an overview of the presence, areal extent and stratigraphic level of the various sandstone bodies within the six units.

4.3 | Sandstone connectivity

Migration of CO_2 out of the reservoir into sandstones within the Seal Interval (termed 'primary migration') depends on the presence, lateral extent, integrity and thickness of the mudstones between them. Once migrated from the reservoir, CO_2 will: be trapped in sandstones in the Seal Interval; migrate vertically through cross-cutting of the stratigraphy due to poor seal integrity or migrate up-dip in foreset sandstones (termed 'secondary migration'). To have a complete secondary migration route, the Overburden Interval migration path must extend through the full interval. Sandstone connectivity (and thus potential primary and secondary migration)

is analysed by assessment of the spatial proximity of sandstones, and the thickness and extent of intervening mudstones (Figure 2b). This was achieved using amplitude and thickness maps of the intervening mudstones, and vertical seismic sections with well data to identify connection points among the reservoir, Seal Interval and Overburden Interval sandstones.

4.4 | Regional shallow gas seismic assessment

Migration of shallow gas can present evidence of fluid migration pathways, which could be re-used by injected CO_2. To identify shallow migration pathways, gas-like seismic expressions were identified in the seismic data. Gas may be in-place due to bacterial reduction in organic matter (biogenic) or it may have migrated up from a deeper source (thermogenic) (Floodgate & Judd, 1992).

The presence of gas causes a large reduction in density and acoustic velocity of the host strata, with low gas saturations (ca. 15%), reducing P-wave velocity by ca. 50% (Constable, 2010). Sandstones here mainly present 'soft' tops, thus the presence of gas acts to amplify the negative amplitudes. Such high-amplitude reflection responses can attenuate the seismic signal and reduce the available energy for further downwards transmission, resulting in acoustic turbidity directly below (Judd & Hovland, 1992;

TABLE 1 Sandstone presence classification scheme

Proven	
Sandstone body identified in geological well data and could be correlated between two or more wells with the seismic data.	

Probable	
Seismic extrapolation of a 'proven' sandstone beyond well control. Example shows interpretation of the sandstone termination where there is a change in amplitude and/or reduction in thickness.	

Possible	
Sandstone identified using similar seismic response to 'proven' sandstones, i.e. high-amplitude soft response or high sweetness top with hard response base, or features identified from seismic geomorphological analysis.	

Note: The assignment of each of the three categories is applied to the map in Figure 7. Sweetness colour bar from Crameri (2021).

Abbreviations: AI, acoustic impedance; SS, sandstone.

Myung & William, 2001). This is not always the case, attenuation below the Peon discovery is small, but it is typical where gas is present in several layers (Arntsen et al., 2007). Velocity pull-downs and low-frequency shadows (Han, 2019) are other diagnostic features of gas in-place. Pockmarks may also be present above shallow gas accumulations and form when gas escapes to the palaeo-seafloor (Hovland et al., 1984).

The following methods were used to identify potential gassy signatures on a regional scale, and subsequently assessed at a local scale. Assessment of negative seismic amplitudes was primarily used to identify possible gas indications, whereby minimum amplitudes (i.e. high negative amplitudes) above a threshold of −50,000 were mapped. This number was calibrated against the Peon gas discovery which is directly overlying the URU (top amplitude of −50,000 to −130,000). The minimum amplitude was extracted from two windows: 20 m above and below the URU, and from 20 m below the URU to the Top Utsira Fm. The window surrounding the URU is considered independently because the URU can act as a seal for trapped gas at the clinoform truncations (and also overpressure; e.g. well NO 35/9-4S), or it may define the base of gas-prone glaciogenic units (e.g. Peon gas discovery) (Chand et al., 2012). The minimum-amplitude extractions were used in conjunction with the variance extraction for the whole Overburden

interval, which highlights acoustic disturbances that could be interpreted as seismic chimneys (low trace-to-trace correlation). Anomalous features highlighted on this regional seismic amplitude and variance map were individually assessed to determine the likelihood of the feature being gas (Section 5.6), however, without firm evidence of gas in petrophysical and drilling data from wells, it is challenging to provide a confident shallow gas interpretation.

Identification of migration itself can be more cryptic, but acoustic turbidity, chimneys, faults and pockmarks are the available evidence in seismic data (Cartwright et al., 2007; Hovland & Judd, 1988). Gas can migrate through the overburden in two ways: (a) direct vertical migration, crosscutting the stratigraphy, causing seismic chimneys and pipes (Cartwright et al., 2007; Løseth et al., 2009); (b) migration up-dip following the stratigraphy, causing amplitude anomalies where sealed and pockmarks on palaeo-seabed horizons (e.g. the URU). It should be noted that there are other geological features that produce similar seismic features as described above, such as: glacial tunnel valleys causing underlying velocity disturbances (Huuse & Kristensen, 2016), pockmarks caused by de-watering (Andresen & Huuse, 2011) or iceberg pits (Brown et al., 2017), and amplitude anomalies from tuning (Barrett et al., 2017) or lithology effects (Bacon et al., 2003).

5 | RESULTS

5.1 | Stratigraphic framework

The studied stratigraphic interval extends from the Top Utsira Fm., or Top Hordaland Group Unconformity for areas where the Utsira Fm. is absent (THGU), to the URU, above which there is a major change in sedimentation pattern (Ottesen et al., 2014). The Utsira Fm. boundaries have been reinterpreted since their original definition (Isaksen & Tonstad, 1989), and therefore vary between well completion reports (Eidvin et al., 2013; Rundberg & Eidvin, 2005). For this study, the most recent Utsira Fm. definitions were used and the interpretations from published seismic sections were extrapolated across the study area (Eidvin & Rundberg, 2001, Eidvin et al., 2013, 2014; Gregersen & Johannessen, 2007; Løseth et al., 2013; Rundberg & Eidvin, 2005). The majority of the top Utsira Fm. is expressed as a high-amplitude soft reflection (Figure 2c) and can be correlated with confidence. In some areas, the top Utsira Fm. is more speculative, for example, in the Tampen Spur area, due to the low acoustic contrast with the overlying succession (Øygarden et al., 2015).

The studied interval has been sub-divided into six seismic stratigraphic units, with each unit split into a west (W) and east (E) sub-unit representing the two prograding shelf systems: one from the ESP in the southwest and one from the Norwegian Margin (NM) in the east (Figure 4). Both systems exhibit typical clinoform geometries with high-amplitude, semi-continuous, basinward-dipping foreset reflections. The east and west systems (and possible extrudites in the north) interact in the centre of the basin (termed the 'Interaction Zone') (Figure 6). The orientation of the ESP shelf break in relation to the NM is parallel in the south (Figure 4a), oblique in the centre (Figure 4b) and perpendicular in the north (Figure 4c) of the study area. This results in variable interactions between the systems from the south to the north.

In the south, where the palaeo-shorelines were parallel to each other (north–south orientation), there was direct interaction of the two shelf systems (Figure 4a). The earliest clinoforms to post-date the Utsira Fm. downlap the THGU (Unit 1E). Progradation further into the basin (ca. 20 km) led to direct downlap onto the Utsira Fm. (Unit 1 and early clinoforms of Unit 2E, Figure 4a). There is no apparent interaction with the coeval clinoforms from the ESP until the deposition of the later clinoforms of Units 2. Clinoform bottomsets in Units 2 and 3 interfinger near the centre of the basin, where chaotic, low-amplitude seismic signatures are apparent. Subsequent deposition was generally dominated from the NM, with Unit 4E clinoforms downlapping directly onto Unit 3W clinoforms. Unit 5 is characterised by low-amplitude, noncontinuous, homogenous reflections, restricted to the centre of the basin. Unit 6E comprises west-dipping clinoforms that have a foreset height up to 80 m, whereas Unit 6W is characterised

by near-horizontal reflections, which appear to truncate Unit 1W-3W clinoform topsets. The clinoform topsets in Units 1E-4E are truncated by the URU (Figure 4a).

Towards the basin centre, palaeo-shorelines were obliquely orientated and there is a different interaction between the two systems (Figure 4b). As the Top Utsira Fm. deepens towards the north and the basin widens (from ca. 80 to ca. 140 km), flat-lying, continuous reflectors connect the two coeval clinoform sets of Unit 1 and separate the Utsira Fm. from Unit 2. This contrasts with the southern study area (Figure 4a), where such bottomsets are not apparent, allowing Unit 2 to be in direct contact with the Utsira Fm. Units 3–6 exhibit similar architecture in the central region as in the south on a regional scale, except for the preservation of Unit 4E and 5E clinoform topsets.

The northern study area is in a distal position from the ESP allowing the eastern clinoforms to dominate the stratigraphy (Figure 4c). The eastern clinoforms have a greater foreset height (ca. 450 m) relative to those in the central study area (ca. 300 m). The thickness of Units 5 and 6 is also greater (400 and 300 m, respectively), relative to the central study area (200 and 300 m). The ESP shelf break is orientated northeast–southwest in the centre of the study area, and therefore the distal bottomsets from the western clinoforms trend perpendicularly to those from the eastern clinoforms (Figure 4c). Here, clinoform bottomsets of Units 1–4 onlap mounded features from below.

5.2 | Seal geometry

To understand the regional variability of the seal geometry, the Top Utsira Fm. surface was raised 50 m to create the 'Top Seal Interval' surface, onto which seismic amplitudes were extracted (Figures 4 and 5a,b). The colour bar was adjusted to accommodate for the regions of low amplitude, since it is the geometry and not absolute amplitude that is of interest. Alternating positive-negative amplitude bands (peaks and troughs) are apparent where the Top Seal Interval surface slices dipping stratigraphy, such as clinoform foresets. Broad areas of a single polarity are apparent where the surface intersects stratigraphy approximately parallel to the Top Utsira Fm., such as clinoform bottomsets (Figure 5a,b).

Intersection of foresets (dipping stratigraphy) is apparent primarily in the south across both shelf systems, which suggests the bottomset succession (parallel stratigraphy) is either not present or <50 m thick above the Utsira Fm. There is direct contact between west-dipping foresets and the Utsira Fm. in the southeast of the study area (Figure 5c). Intersection of parallel stratigraphy is apparent towards the north of the study area, primarily in Blocks 34/9, 34/12 & 30/3 (Figure 5b). This parallel-bedded area ('Basal Upper Pliocene' in Eidvin & Rundberg, 2001; 'Shale drape' in
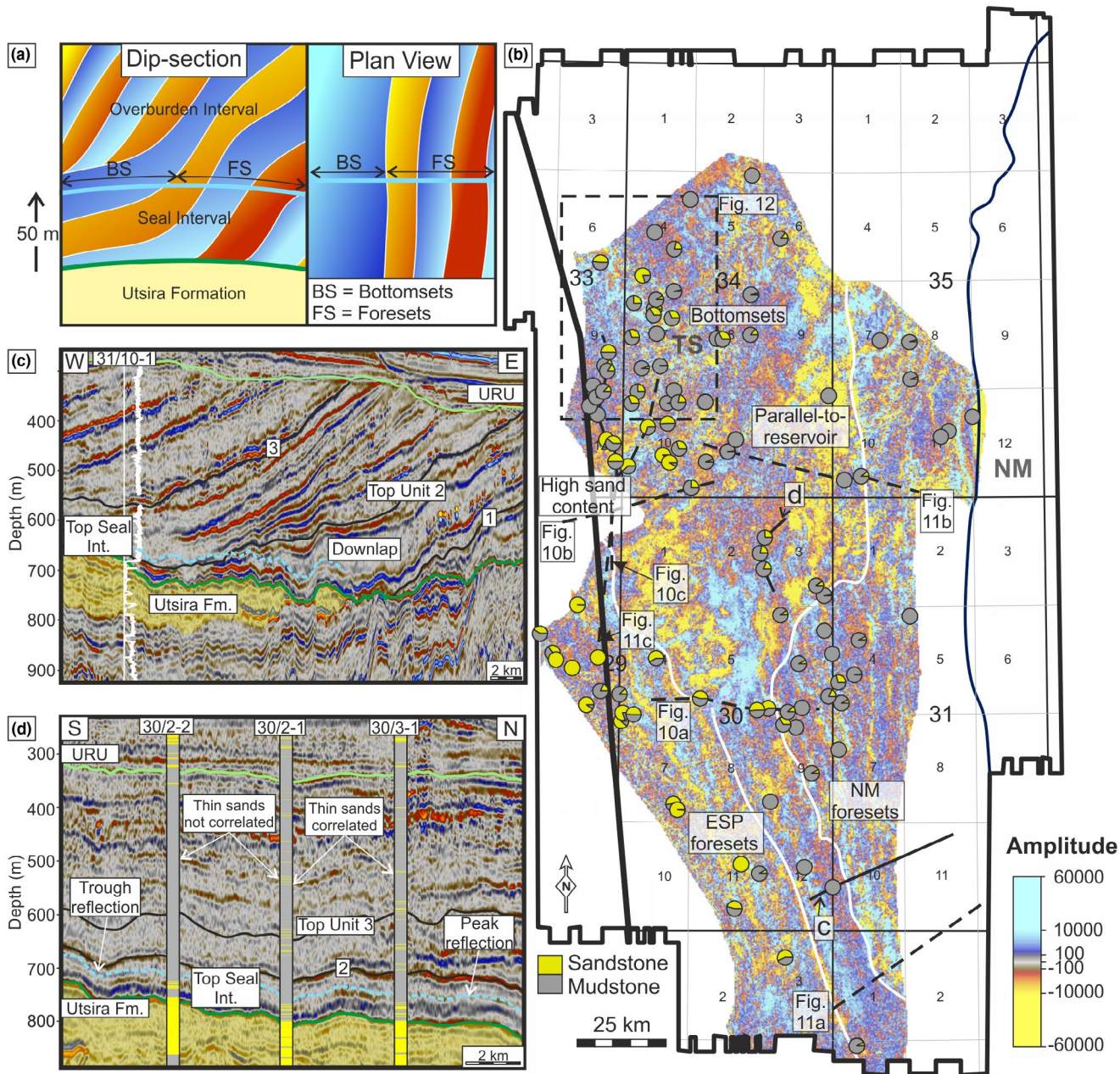
FIGURE 5 Geometry and sandstone percentages of the Seal Interval (<50 m above Utsira Fm.). (a) Schematic seismic image to show how the amplitude extraction through a slice of the clinoforms reveals the intersection of dipping or flat-lying beds in the Seal Interval. (b) Top Seal Interval surface (Top Utsira Fm. surface brought up 50 m) with seismic amplitudes, overlain by well lithology percentages within the Seal Interval. Stratigraphy is dipping (foresets intersected) in the areas towards the south and east, and flat-lying (parallel to the Top Utsira Fm.) in areas towards the north. White lines indicate the inferred boundary between foresets and bottomsets. (c) Seismic dip-section to show the direct downlap of the NM clinoform foresets onto the Utsira Fm. in the southern region. (d) Seismic strike section through the wells penetrating bottomsets in the central study area (Blocks 30/2 & 30/3) to show thin sand beds towards the base of the Seal Interval overlain by a thick mudstone succession. White lines show gamma-ray response from 0(L) to 150(R) api

Gregersen & Johannessen, 2007) is extensive (>3,000 km^2) and only connected to correlative foresets on its eastern margin. Some gradual polarity transitions occur across the surface in this area due to small thickness variations of the bottomsets. In the Tampen region, the surface mainly intersects parallel-to-reservoir stratigraphy, but it has a noisy appearance in plan view due to the chaotic seismic reflections

and mounds in the area. Mounds reach 150 m in height and are therefore cut by the top Seal Interval surface (Figures 4c and 5b).

Well sandstone percentages within the Seal Interval have been overlain onto the map in Figure 5b to highlight the sandstone content (and therefore migration potential) of the clinoforms. The foresets within the Seal Interval are sand
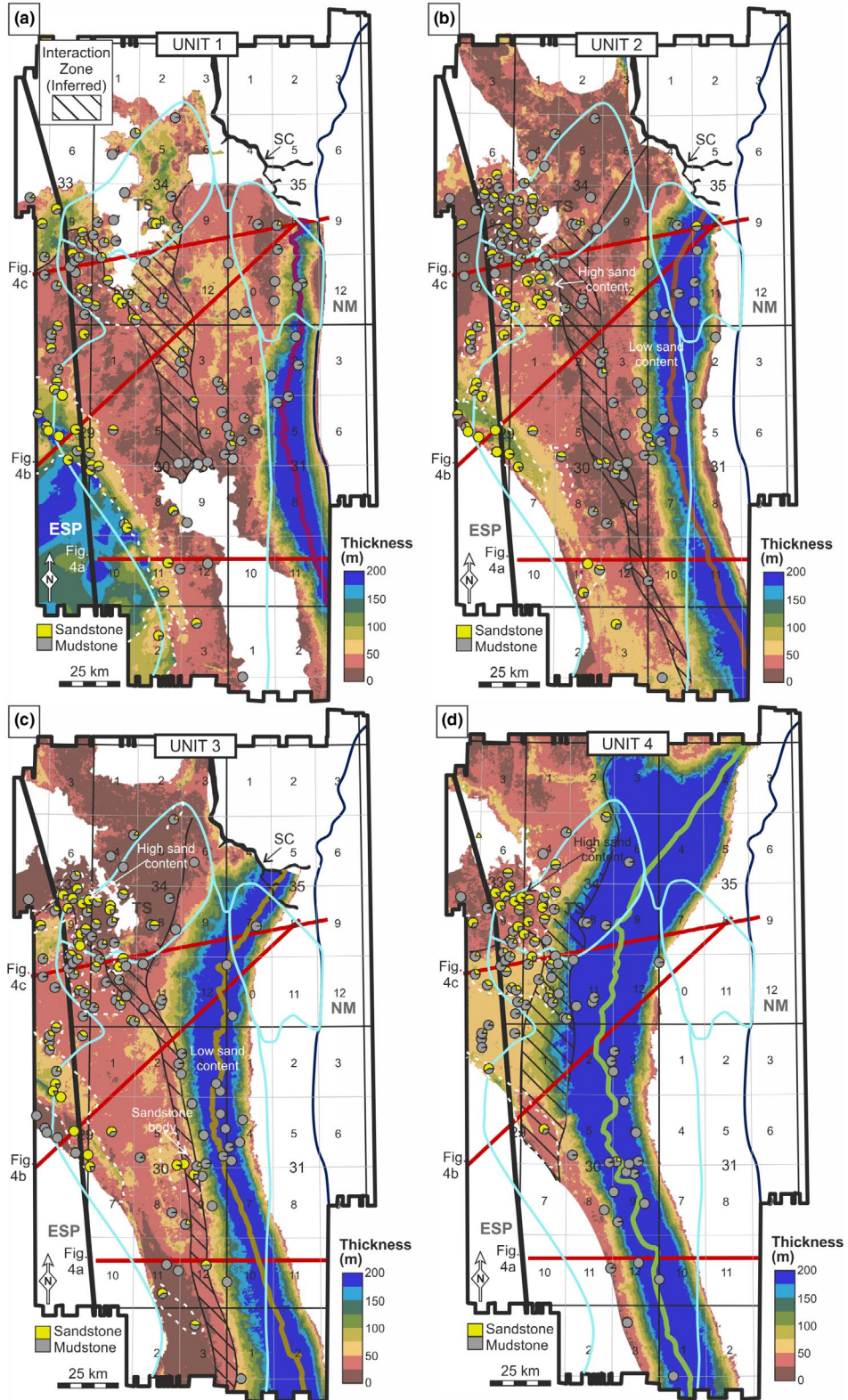
FIGURE 6 Seismic unit thickness maps with unit lithology percentages from wells overlain. (a) Unit 1; (b) Unit 2; (c) Unit 3; (d) Unit 4; (e) Unit 5 and (f) Unit 6. The Utsira Fm. outline is in light blue on all maps. The approximately north–south trending thick line on the right of each image (coloured as per the unit in each) indicates the eastward limit of the fully preserved interval of each unit. Beyond this, the URU has truncated the unit and thicknesses are reduced from erosion. White dashed lines represent extent of major 'proven/probable' individual sandstone bodies. Black hatched section is the 'Interaction Zone' where the depositional systems meet. SC, Sunnfjord channel, from Løseth et al. (2020)
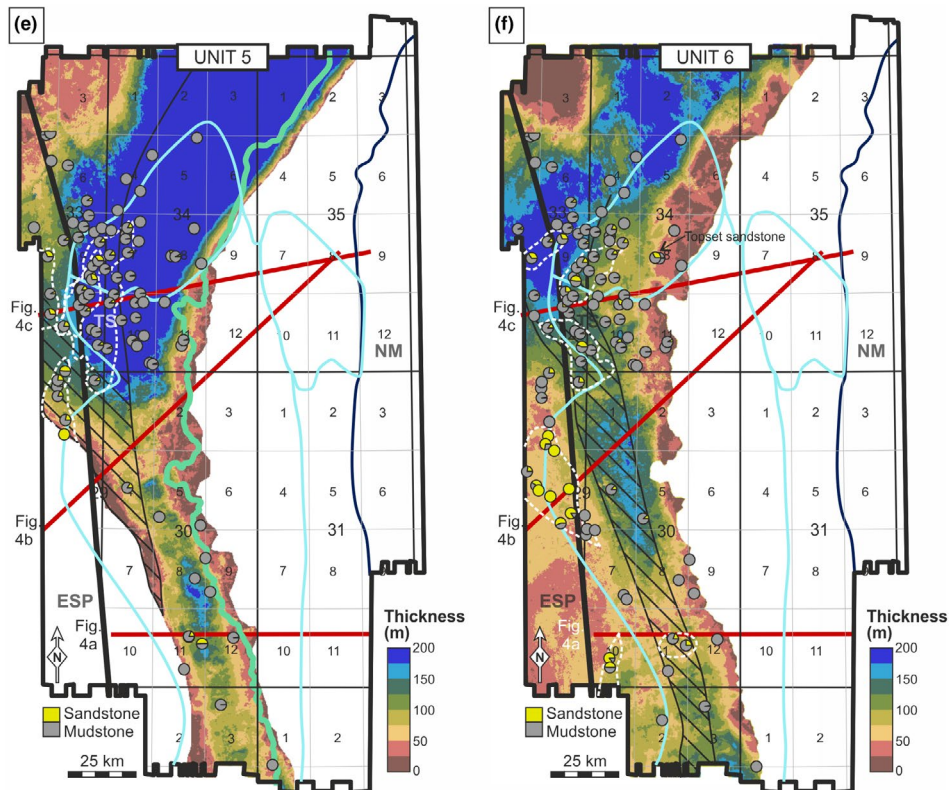
FIGURE 6 (Continued)

rich (>50%) from the ESP (western system), but sand poor (<10%; except for a few wells in Blocks 30/6 and 31/4, where sandstone content is <25%) from the NM (eastern system) (Figure 5b). The different depositional system types can be attributed to this lithological contrast; sediments from the east are derived from a glacial system and mainly deposited through glaciogenic debris flows (Løseth et al., 2020), whereas sediments from the west are derived from a nonglacial, fluvio-deltaic system and deposited through sand-rich turbidity currents. There are high sand percentages in the wells in the Tampen Spur region, the distribution of which is discussed in Section 5.3. The parallel unit in the central and northeast study area is mainly mudstone dominated (>95%) except for a cluster of wells in Blocks 30/2 and 30/3, where sand percentages reach up to 25%. However, these sandstones are positioned at the base of the 50 m interval as <1–8 m sandstone beds and are overlain by flat-lying mudstones (Figure 5b,d).

5.3 | Sandstone presence

Seismically resolvable sandstones (top = red reflection, denoting a soft response; base = blue reflection, denoting a hard response) are encountered in wells in all six units across the study area (Figures 6 and 7). Here, focus is on the sandstones in close vertical proximity to the reservoir (Units 1–4).

In the topset-to-foreset region of the ESP, Unit 1W is thickest (up to 200 m) and has wells with >50% sandstone percentages (Figure 6a). On the basin floor, where the unit is thinner (<50 m), wells with high sandstone percentages (>50%) are focused in the southern Tampen Spur region (Figure 6a). Isolated wells in the northern Tampen Spur region have high sand content (Blocks 34/8 & 34/4; Figure 6a), with high-amplitude soft reflections in the thicker part of Unit 1, which indicates possible sandstones in this region (Figure 7). Unit 1E contains >95% mudstone, except for a few wells in Block 31/4 which have sandstone percentages of 15%–40%. However, the individual sandstone beds cannot be correlated between wells and no seismic geomorphologies were identified in this unit (Section 5.4).

In Unit 2W, high (>50%) sandstone percentages and increased unit thickness from ca. 25 to ca. 75 m is observed in the southern Tampen Spur region bottomsets (Figure 6b). This represents a sandstone body that is correlated between wells ('proven' in Table 1). Its northern and eastern extent are defined by a sharp reduction in sand content in wells, and its southern and western extent rely on interpretation based on a reduction in unit thickness or dimming of amplitudes and sweetness. The sandstone is proven to extend 35–40 km east–west and 25 km north–south (Figure 6b), but through extrapolation of the seismic signature it could reach >70 km east–west and >50 km north–south ('probable' in Table 1; Figure 6b). The sand content of wells in Unit 2E is similar to
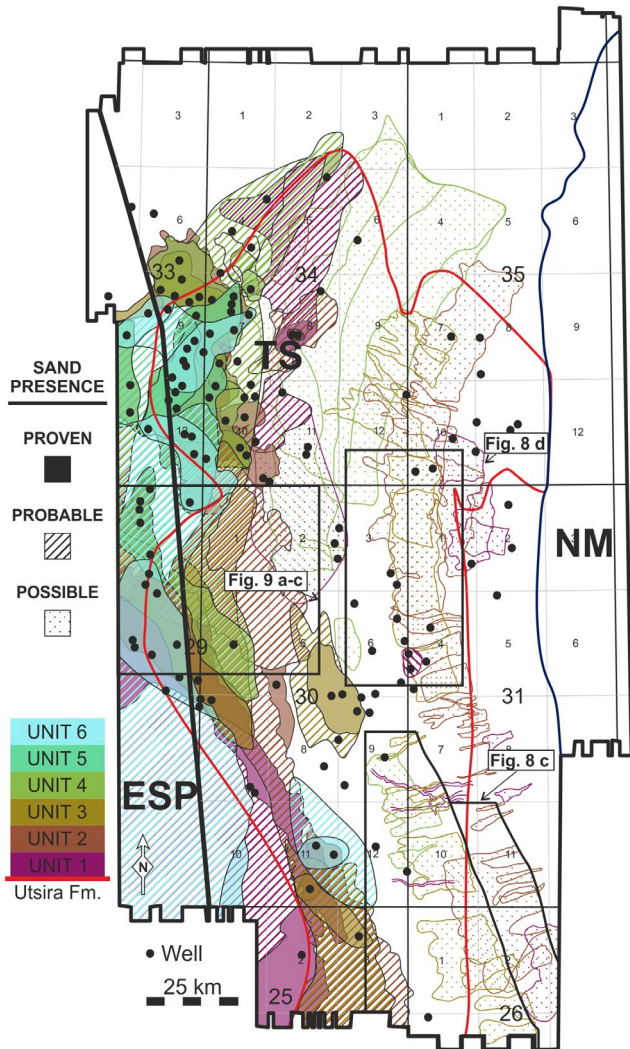
trend) and is 30–40 km long and 10–15 km wide (Blocks 33/6 & 33/9; Figure 6c). Its southern limit extends beyond the study area. There are additional thinner and smaller sandstone bodies in Unit 3E in the Tampen Spur region, positioned stratigraphically higher. The limits of the sandstone body in the central study area are demonstrated by a sharp decrease in well sand content and thickness to the west, and by a reduction in amplitude and sweetness strength to the north and south. Unit 3W wells are mudstone dominated.

In Unit 4W, a laterally extensive, seismically resolvable sandstone body is present in the central part of the Tampen Spur region bottomsets (Figure 6d). This sandstone has a strong seismic character allowing clear definition of its lateral boundaries. In the southern Tampen Spur area bottomsets, sandstones in Unit 3 continue into the basal stratigraphy of Unit 4 (basal 20 m), which are overlain by mudstone-dominated stratigraphy. Due to the large unit thickness (>200 m), the overall sand content in the wells for Unit 4 is low (ca. 20%) (Figure 6d).

Multiple thin sandstones are identified in wells at different depths in the relatively thick Unit 5, where the thickness of the unit exceeds 500 m (wells in Blocks 31/9 & 31/12 in Figure 6e). Overlying this, and confined to the west of the study area, Unit 6 has multiple localised seismically resolvable sandstone bodies (Figure 6f). In summary, evidence suggests that the greatest sandstone presence in the main prograding clinoform units (Units 1–4) is in the west, primarily in two regions: (a) on the shelf and proximal slope of the ESP, and (b) at the base-of-slope in the Tampen Spur region (Figures 6 and 7). The eastern clinoforms (Units 1E-5E) are mudstone dominated, except for a few wells in the centre of the basin (Block 31/4).

5.4 | Seismic geomorphology

Seismic geomorphological analysis (e.g. Posamentier, 2004) was undertaken, in order to identify 'possible' sandy features on the slope and basin floor (Figures 8 and 9). Two areas were of focus: (a) the southern and central NM clinoforms, where there is limited well penetration; and (b) up-dip of the Tampen Spur region, where sandstones have been identified (Section 5.3). Using a suite of seismic volume attributes (maximum negative amplitude, sweetness, variance and frequency decomposition), narrow, elongate features with variable sinuosity were identified, trending down-dip towards the centre of the basin from both source areas. In some places, at their down-dip termination, they appear to splay. The features are interpreted as submarine channels and lobes.

Wells that penetrate the NM clinoform foresets are mudstone dominated in all six units, except for a few thin (1–5 m) sandstones that cannot be correlated using the seismic data. For the southern NM clinoforms, frequency decomposition
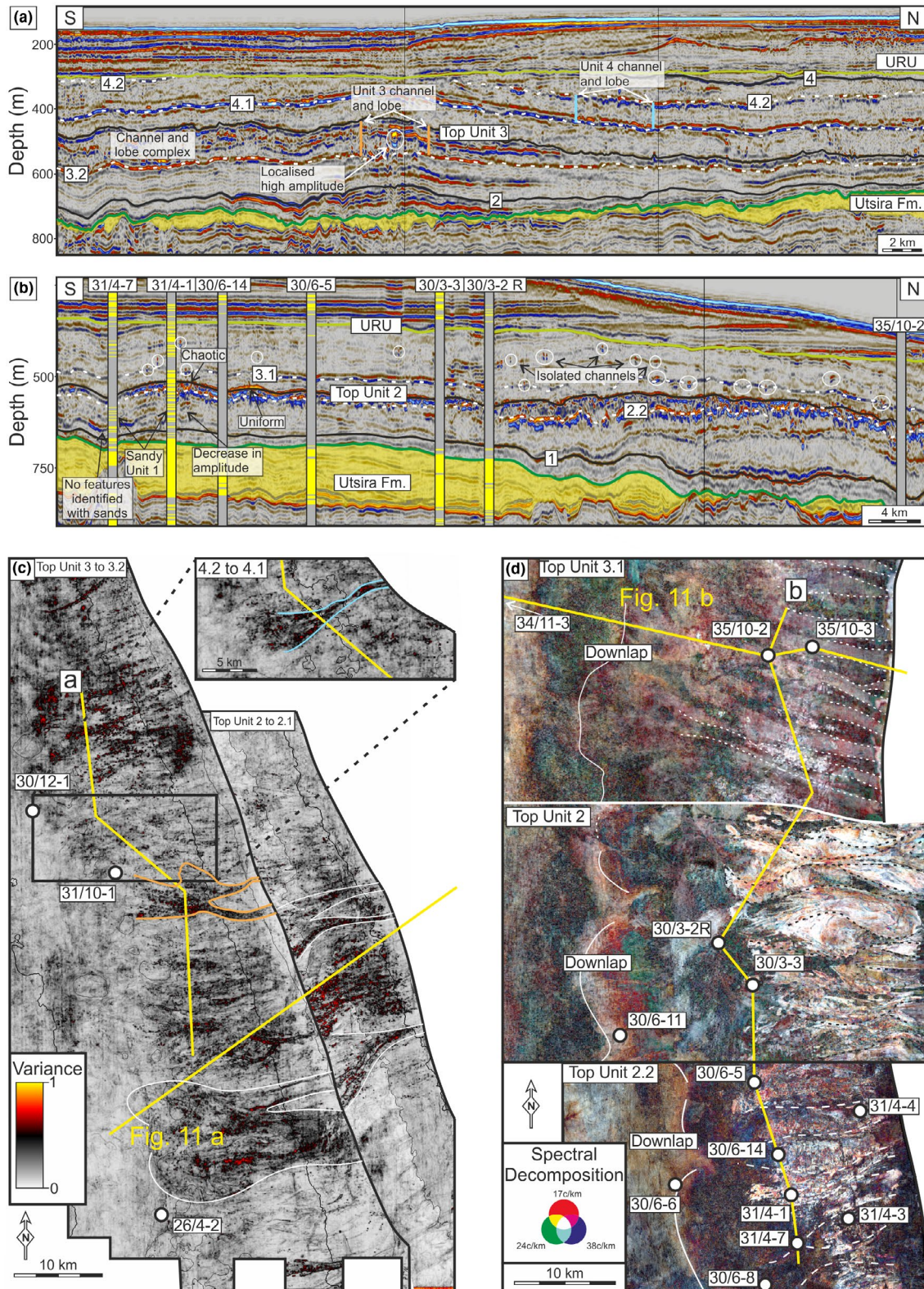

FIGURE 7 Seismically resolvable sandstone body presence for each of the six units. Sandstone bodies were shaded using the 'proven' (with well data), 'probable' (seismic extrapolation from 'proven' sandstones) and 'possible' (seismic character of 'proven' sandstones but no well penetration) sandstone presence classification (Table 1), and coloured according to their unit. The sandstone bodies in the NM clinoforms are interpreted as 'possible' from seismic geomorphologies as few thin sandstones are encountered. ESP, East Shetland Platform; NM, Norwegian Margin; TS, Tampen Spur. Colour bar from Crameri (2021)

that in Unit 1E, being primarily mudstone dominated, except for wells in Block 31/4.

In Unit 3E, two thick (>50 m), high sandstone percentage (> 50%) regions are observed in the clinoform bottomsets: (a) the southern Tampen Spur region in Block 33/9; and (b) the central study area in Blocks 30/5 & 30/8 (Figure 6c). For both regions, the high sandstone content comprises individual sandstone bodies that are correlated between wells ('proven'). In the southern Tampen region, multiple, vertically stacked individual sandstone bodies are mapped. The largest sandstone body has an elongated geometry (northeast–southwest

FIGURE 8 Features identified through seismic geomorphological analysis of the Norwegian Margin (NM) clinoforms. (a) Seismic strike section through clinoforms in the southern region, highlighting the channel and lobe complexes within Units 2 & 3, shown in 'c'. White labels indicate unit and intra-unit tops. Orange and blue lines indicate extent of features highlighted in 'c'. (b) Seismic strike section of clinoforms in the central region, highlighting the Unit 2 channel complex, isolated Unit 3 channels and the high sand content wells, shown in 'd'. No seismic geomorphologies were identified in Unit 1 and basal section of Unit 2 in this region. (c) Interval variance extraction for Unit 2 (Top Unit 2–2.1), Unit 3 (Top Unit 3–3.2) and Unit 4 (4.2–4.1). (d) Surface extraction of frequency decomposition for Top Unit 2, 2.2 and 3.1. 'c' & 'd' highlight the presence of channel-lobe systems that could be sand filled (mapped as 'possible' sandstones in Figure 7). Locations of 'c' & 'd' shown in Figure 7
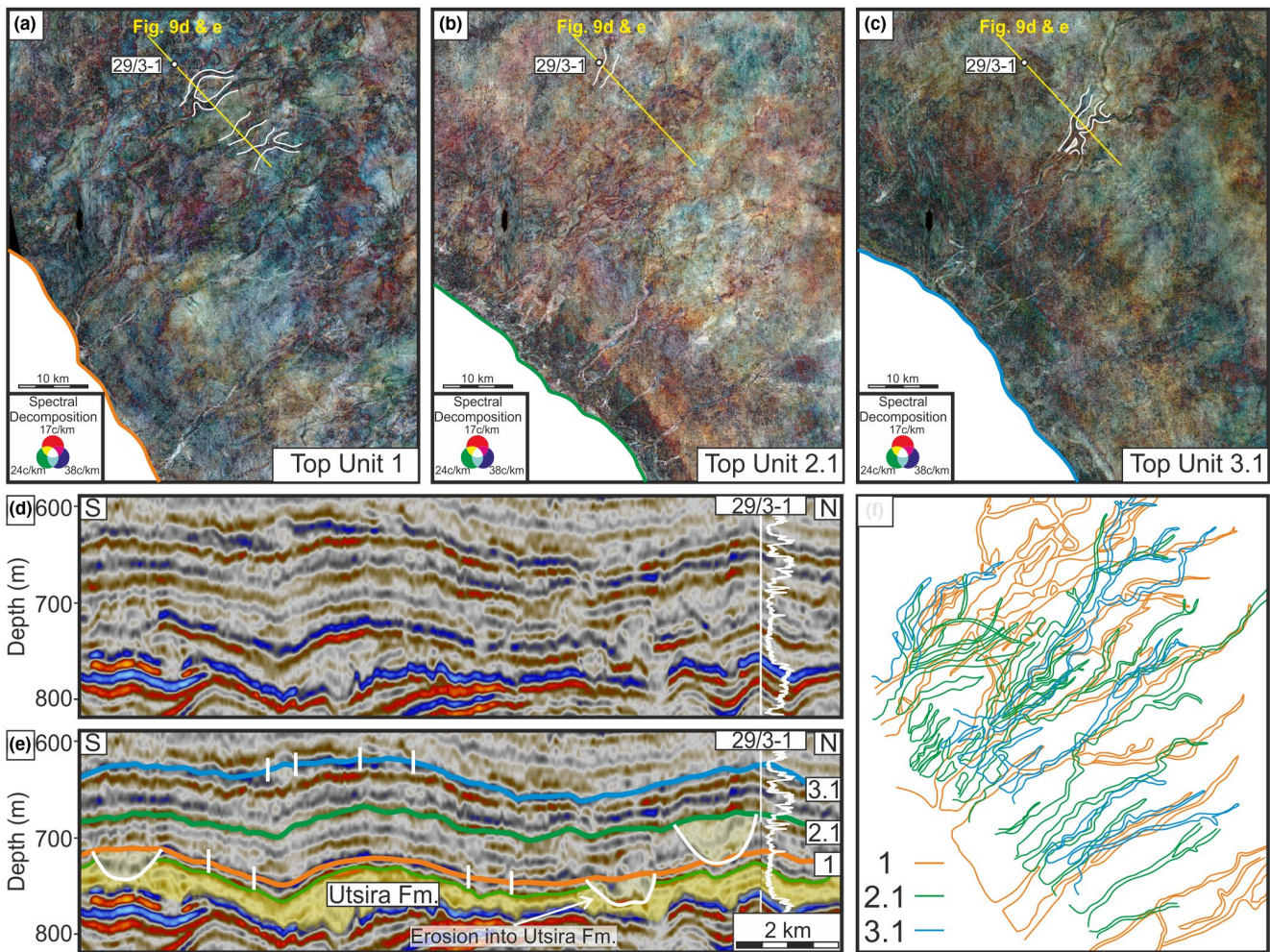
FIGURE 9 Channels identified through seismic geomorphological analysis in the East Shetland Platform (ESP) clinoform foresets. (a–c) Frequency decomposition of three horizons (Top Unit 1, Top Unit 2.1 and Top Unit 3.1) within a 100 m interval. White outlines highlight channels shown in cross-section in 'e'. (d and e) Seismic strike section (d) with interpretations (e) of the three surfaces ('a'-'c'), highlighting the erosive geometry of the channels and their seismic character. White line shows gamma-ray response from 0(L)-150(R) api. (f) Overlay of the channels from surfaces 'a'-'a', showing their cross-cutting geometries, suggesting possible vertical connection. Locations of 'a'-'c' shown in Figure 7

maps reveal channels on the foresets and lobes towards the base-of-slope, which have a width of 6–26 km. The features are vertically stacked over ca. 100 m towards the tops of Units 2, 3 and 4 (Figure 8c). In strike section, they have a chaotic seismic signature with localised high negative amplitudes (Figure 8a) and are individually mapped (Figure 7).

In the central study area, the NM foreset channels have two architectural styles. In Unit 2, they are comparable to those in the south; high-amplitude, vertically stacked, <4 km width and sinuous with clear lobes at the base of slope (e.g. Top Unit 2 in Figure 8b,d). These are interpreted to be localised channel complexes (glaciogenic debrites; Løseth et al., 2020). At other stratigraphic levels, channels are less sinuous, 1–3 km in width and are more isolated. In strike section, they appear as high negative amplitude, single reflections among low-amplitude surroundings (white circles in Figure 8b). Coeval, down-dip lobes are not always

observed (Top Unit 2 in Figure 8d). Relative to the southern NM channel-lobe systems, the central NM systems are more amalgamated, which makes identification of individual, full channel-lobe systems challenging. Hence, rather than mapping individual elements, they are captured as broad complexes in Figure 7. Most wells penetrating these complexes show a mudstone succession, however, two wells show high sandstone content (NO 31/4-1 & 31/4-7; Figure 8b). The fill of these features beyond the vicinity of well control is uncertain. The top reflection becomes slightly chaotic where there is evidence of sandstone from wells (Figure 8b). In map view, there appears to be a higher-frequency content in the sandstone features relative to the mudstone features (Figure 8d), although this is not always the case. These wells also have a high sandstone content in Unit 1, however, no seismic geomorphological features were identified at that stratigraphic level.

Channels are also apparent on the western side of the basin (central and northern areas of the ESP) in Units 1–4, as low-amplitude features that appear to erode into underlying mudstones (positive amplitude, blue horizon) and are interpreted to be sand filled (Figure 9). In the north, the channels are more sinuous and some extend further into the basin (>50 km) relative to the NM foreset channels. There is only one well in this region (NO 29/3-1), which has a stacked sandstone–mudstone succession. Three seismic horizons (mudstone beds) within 100 m above the Top Utsira Fm. underwent a frequency decomposition extraction to highlight the erosive and amalgamated channels that cut through the mudstones (Figure 9a–c). The channels are vertically stacked, with widths <1 km and thicknesses <50 m (Figure 9f). In strike section, their character is variable. Some channels appear as areas with dimming of a single positive amplitude reflection (Top Unit 3.1) and larger channels appear as erosive surfaces that are onlapped and filled by subsequent stratigraphy (Top Unit 2.1) (Figure 9d,e). In some places, channels erode into the underlying Utsira Fm. (Top Unit 1) (Figure 9d,e), which suggests vertical connectivity. No distinct lobe geometries are apparent in attribute maps, rather, these channels terminate downdip in the sandy bottomsets of Units 1–3 clinoforms in the Tampen Spur region.

5.5 | Sandstone connectivity

In the main clinoform building units (Units 1–4), seismically resolvable sandstone bodies in the clinoform bottomsets are penetrated by wells on the western side of the study area (Section 5.3). Additional 'possible' (Table 1) sandstone bodies have been identified through seismic geomorphological and attribute analysis of the clinoform foresets of both prograding systems (Section 5.4). For up-dip migration, sandstone 'stringers' or channels identified in the foresets would have to be connected to correlative sandstones downdip in the bottomsets, connect vertically to underlying sandstone bodies, or directly downlap the Utsira Fm. Sandstone connectivity is analysed by: (a) assessing the potential for primary migration of CO_2 from the Utsira Fm. to Seal Interval sandstones; and (b) assessing the potential for secondary migration through clinoform foreset Overburden Interval sandstones.

5.5.1 | Utsira Fm. to Seal Interval sandstones connectivity (primary migration)

Seal Interval, bottomset sandstones are primarily encountered in two areas: the central-southern part of the basin and in the Tampen Spur region (Figure 7). The former consists of a regionally extensive sandstone (ca. 1,050 km^2 'proven' and 'probable' area) in Unit 3 that reaches thicknesses of 40–50 m in six wells in Blocks 30/6, 30/8 and 30/9. This sandstone is sourced from the ESP and thins towards the east, onlapping the NM clinoforms (Figure 10a). In the deeper basin there is a 30-m-thick mudstone buffer separating the sandstone from the underlying Utsira Fm. (well NO 30/5-2; Figure 10a). The mudstone layer is represented by a high-amplitude positive response at its top and a high-amplitude negative response at the basal contact to the Utsira Fm. Amplitudes dim and reflections become more chaotic up-dip towards the west, which reflects a transition from homogenous mudstone to interbedded sandstone–mudstone towards the shelf (5–15 m bed thickness) (well NO 30/5-1), thus increasing the possibility for primary migration in the west (Figure 10a).

In the Tampen Spur region, there are a series of bottomset sandstone bodies (800–1,700 km^2 area proven) separated by mudstone layers in Units 2–4 (Figure 7). For the lowermost sandstone body (Unit 2 sandstone), the buffering mudstone between it and the Utsira Fm. varies in thickness, thinning from ca. 50 m in the east (well NO 34/10-23) to <5 m in the west (well NO 29/3-1) over 20 km (Figure 10b). The seismic data show a reduced amplitude of the clear, positive response at the top mudstone from east to west as the mudstone thins below seismic resolution. The spatial extent of the mudstone and its thickness below 5 m are uncertain, so there could be areas in contact with the Utsira Fm. and therefore an increased risk of primary migration.

Additional sandstone bodies in the Tampen Spur region bottomsets (Units 3 & 4) have been assessed for vertical bottomset-to-bottomset connectivity (Figure 10c). In general, the total thickness of Units 2–4 reduces to the north, as a result of mudstones thinning, whereas sandstones maintain their thickness (Figure 10c). For example, an 80-m-thick mudstone buffer separating a sandstone body at the top of Unit 3 (18 m thickness) from a sandstone body at the top of Unit 4 (15 m thickness) gradually thins to ca. 10 m from well NO 29/3-1 to NO 33/9-3, over 32 km. The seismic response of its top changes from a continuous, high-amplitude positive reflection to discontinuous, low-amplitude reflection as the mudstone thins, before thinning below seismic resolution (e.g. at well NO 33/9-4 in Figure 10c). Hence, connectivity of the Unit 2–4 sandstones is greater towards the north. Overlying the sandstone bodies in Units 2–4 is a thick succession of mud-siltstone with only minor sandstone layers (Units 5 & 6), which limits further vertical migration.

Seal Interval sandstones in the eastern clinoforms are only encountered in two wells in Block 31/4 (Figure 8). No visible connection to the reservoir was observed and no up-dip migration paths in this region in Units 1E and the base of 2E have been identified connecting them through the Overburden Interval.
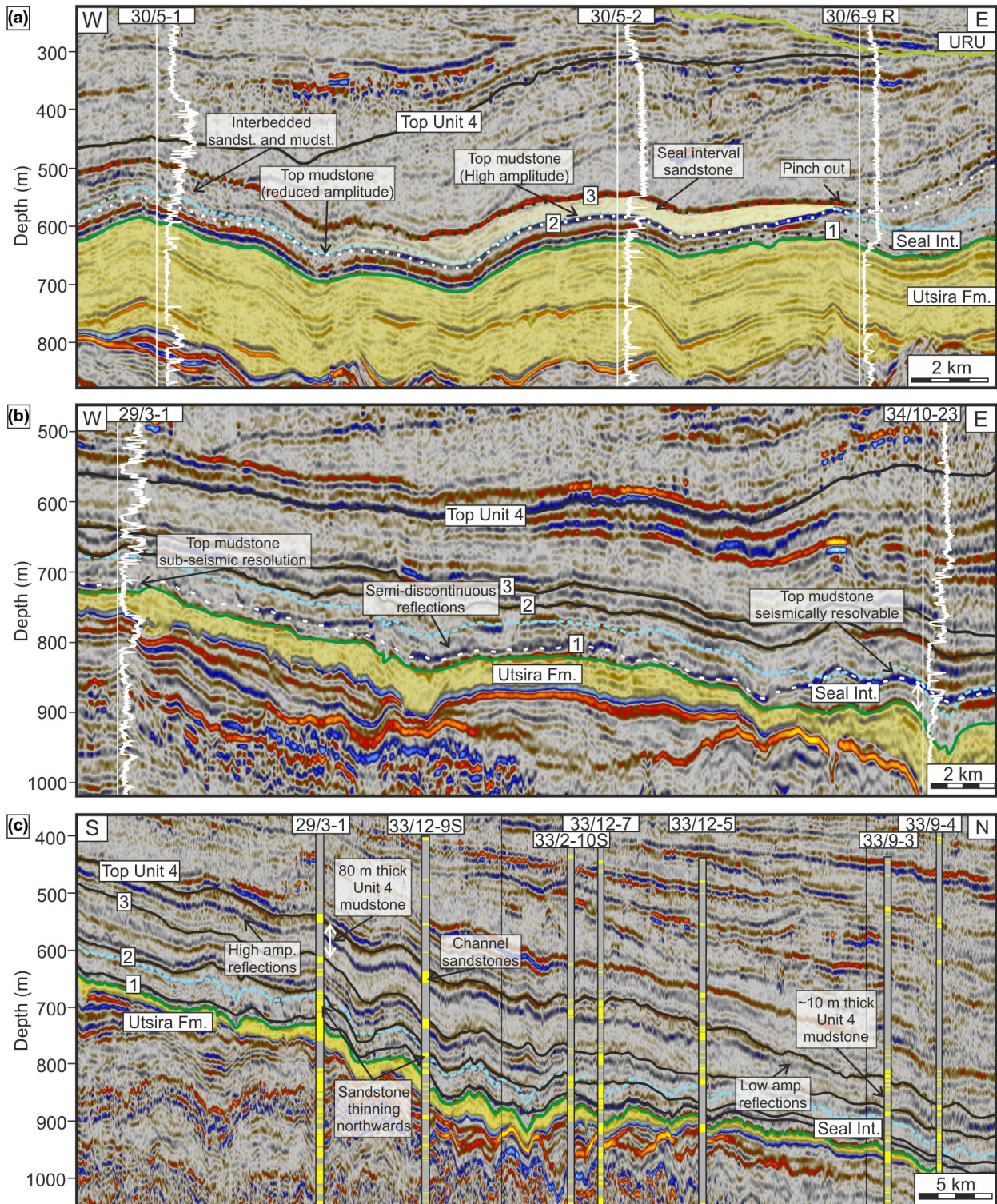
FIGURE 10 Connectivity of the Utsira Fm. to Seal Interval sandstones. (a) Seismic dip-section highlighting the Utsira Fm. and its connectivity with the Unit 3 sandstone body in the central region (Blocks 33/9 & 33/12). There is a lateral transition from a homogeneous intervening mudstone in the centre of the basin to interbedded sandstone and mudstone towards the west. (b) Seismic strike section showing the thickness variability of the mudstone between the Utsira Fm. and the Unit 2 sandstone body in the Tampen Spur region. White line shows gamma-ray response from 0(L) to 150(R) api. (c) Seismic dip section to show sandstone connectivity in the Tampen Spur region. Lowermost sandstones are connected, allowing for primary (vertical) migration. Uppermost sandstones are vertically disconnected by mudstones that thin down-dip (northwards). Correlatable foreset sandstones are apparent (channels), which could allow secondary, up-dip migration pathways. Dark green line = top Utsira Fm.; light green line = URU; blue dashed line = top Seal Interval. Locations of 'a'-'c' in Figure 5

5.5.2 | Seal Interval to Overburden Interval connectivity (secondary migration)

For the channel and lobe features in the foresets of both prograding systems to present a risk of up-dip migration, they would need to be either directly connected to the Utsira Fm., or in connection with the identified clinoform bottomset sandstone bodies. They would also need a porous and permeable sandstone fill, which is proven in the western ESP system, but in most cases for the eastern NM system these features were either not drilled or are mudstone dominated, with only a few exceptions in Block 31/4 (Figure 8b,d).

In the southern NM clinoform foresets, the Unit 2E channel-lobe systems are close to the Utsira Fm. (<40 m above), with the distal part of the foresets directly downlapping onto the Utsira Fm. (Figure 11a). Therefore, there is a possibility for migration directly up the clinoform foresets in this region. The channel-lobe systems identified in Units 3E and 4E (Figure 8c) are located >100 m above the Utsira Fm. in their most down-dip position, with no visible connection observed in the seismic (Figure 11a). Therefore, only poor seal integrity, or localised sub-seismic seal bypass systems (Cartwright et al., 2007; Løseth et al., 2009) would result in migration into these from the Utsira Fm. For the central NM clinoforms, the foresets are separated from the Utsira Fm. by an extensive, 60- to 80-m-thick Unit 1 layer with sub-parallel stratigraphy to the Utsira Fm. (Figure 11b). All the foresets downlap onto this layer, which, from the limited well data, appears to be mudstone dominated in the east (Figure 5; wells NO 35/10-2; NO 35/10-3 in Figure 11b). In the west (Block 34/8), this interval has been cored and contains silty mudstone and fine sand (Eidvin & Rundberg, 2001). However, this is in the Interaction Zone, and the wells are <1.6 km from the nearby mound margins, and therefore the coarser material may be sourced from the ESP or extruded during mound formation (Løseth et al., 2013).

Seismic geomorphological analysis of the ESP reveals the presence of channels that terminate in the bottomsets in the Tampen region (Figure 9). Here, primary migration from the Utsira Fm. to bottomsets is deemed likely through the erosive channels. It is possible that if sandy, the channels could act as fluid conduits up-dip the clinoform foresets to the south, facilitating secondary migration (Figure 11c). In comparison to the NM clinoforms and central ESP clinoforms, the northern ESP clinoforms are longer and have shallower dip (ca. 1° vs. ca. 2.5°), thus potential secondary migration pathways following the northern ESP clinoforms are longer (ca. 60 km) than the NM clinoforms (13–23 km).

Where the ESP and NM clinoforms and associated sandstone bodies interact in the centre of the basin, up-dip, secondary migration paths do not necessarily follow an individual depositional system. This is observed in the northeast Tampen Spur region, where a Unit 4 sandstone body deposited as either a turbiditic sand (Eidvin & Rundberg, 2001) or an extrusive sand (Løseth et al., 2012), is crosscut by a channel from the ESP (Figure 12a). The seismic signature at the top of the channel is a negative amplitude response, similar to the Unit 4 sandstone, suggesting it could be sand filled (Figure 12b). Although there is a buffering and possibly sealing mudstone between this sandstone and the Utsira Fm., there could be a migration route up the margins of mounds, which are in abundance in the Tampen Spur region (Figure 12c). In some cases, the margins could be faulted, but they do not extend above the crest of the mounds, so do not offer complete vertical migration paths.

5.6 | Interpretation of shallow gas and its migration

Migration of shallow gas is important evidence for previous fluid migration pathways. Across the study area, high minimum-amplitude features indicative of shallow gas at the URU appear to be clustered (blue shading in Figure 13a). In the northeast (Blocks 35/1 & 35/2), a large-amplitude anomaly is apparent, which represents the Peon Gas Field. Another large feature (ca. 180 km^2) is positioned near the centre of the study area (Block 34/12). It sits directly above the URU and trends north-south. The feature appears as a high negative amplitude reflection (Figure 11b) and is a good candidate for shallow gas. However, as the trend does not appear to follow the curvature of the clinoform truncations or spatially coincide with sandy features below, it is unclear whether it migrated upwards along the clinoforms or developed in-place. To the west of this, there is a third, smaller high negative amplitude, feature above the Gullfaks field (Block 34/11). The interpretation of gas at the URU at this location is supported by the seabed pockmarks in this area (Løseth et al., 2009). In the south, a series of high-amplitude anomalies are apparent following the trend of the clinoform truncations below the URU (Figure 11a; blue features in Figure 13a,c) and occur in the same area as the channel-lobe complexes identified on seismic attribute maps (Figure 8; grey features in Figure 13c). These amplitude anomalies are also deemed likely to represent trapped gas, which are interpreted to have mainly migrated up the foreset sandstones. Some features have vertical disturbances below them, which could be gas chimneys (proving potential for vertical migration through connected sandstones) or signal attenuation (Figure 11a). Smaller localised amplitude anomalies at the URU are scattered across the study area (Figure 13a). One of these features is associated with pockmarks on the seabed above and has reflection disturbances directly below (Figure 13f). Other examples directly overlay the margins of the deeper mounds (Figure 13g). These amplitude anomalies are interpreted to be pockets of shallow gas at the URU, trapped by the overlying glaciogenic sediments and have associated seismic noise chimneys below causing high variance. Further analysis would be required to fully attribute the noise
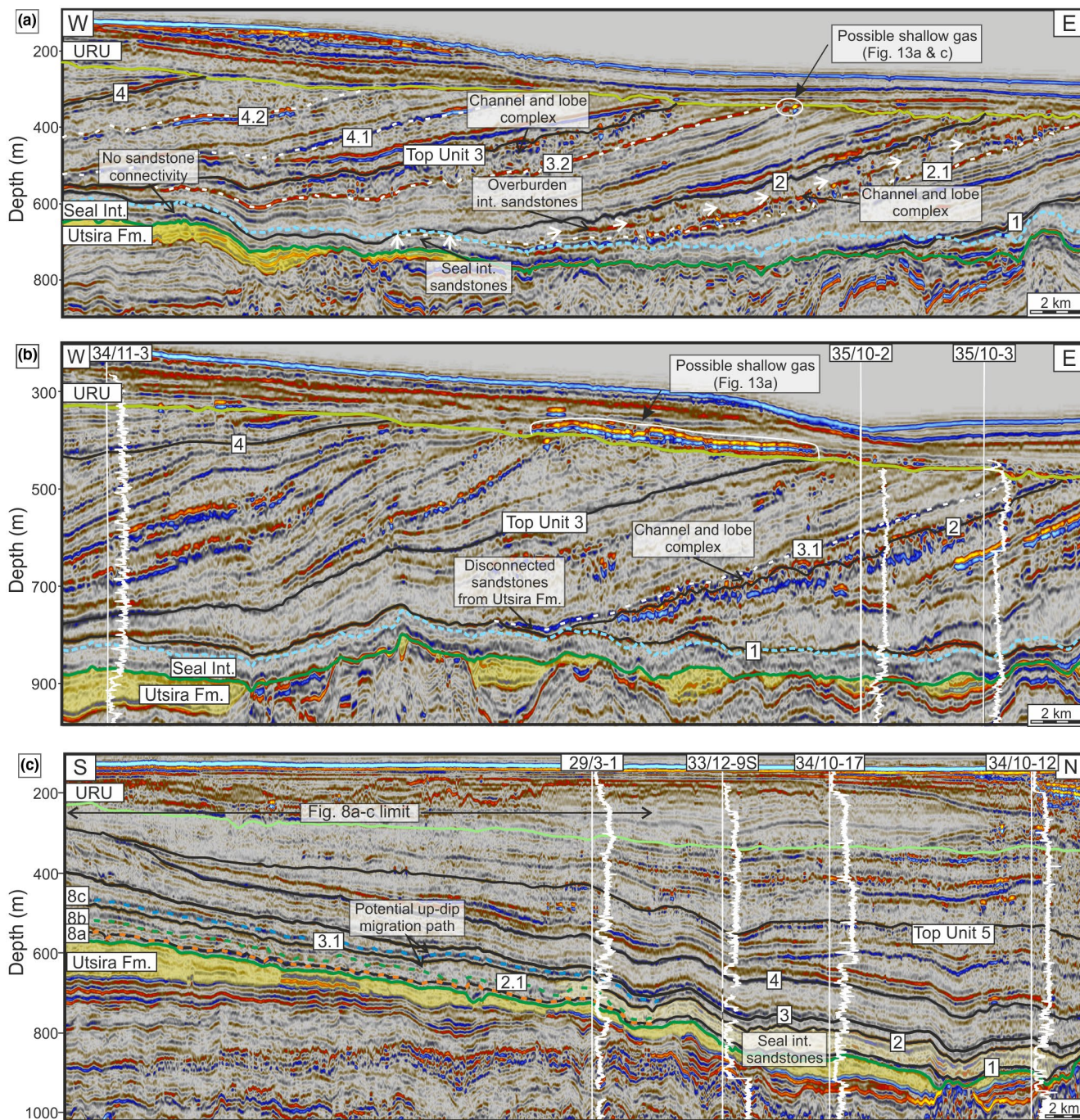
FIGURE 11 Connectivity of the Seal to Overburden Interval sandstones. (a) Seismic dip section to show the potential up-dip migration routes through the NM foreset channels in the southern region that terminate down-dip within the Seal Interval (2–2.1). White arrows indicate potential migration route. (b) Seismic dip section to show the disconnection between NM foreset channels and the Utsira Fm. by flat-lying Seal Interval mudstones in the central region. (c) Seismic dip section to show potential up-dip migration routes in the ESP foresets, highlighting the connection between bottomset sandstones in the Seal Interval (Unit 2) and the Utsira Fm. that promotes primary migration. Potential secondary migration paths are indicated through foreset channel sandstones (Figure 8). White line shows gamma-ray response from 0(L) to 150(R) api. Location of 'a' & 'b' shown in Figure 7 and 'c' in Figure 5

chimneys to attenuation beneath discrete gas accumulations, or disturbances to strata from vertical gas migration. There are few amplitude anomalies at the URU on the ESP. Here, the clinoforms are instead truncated by the flat-lying Unit 6 and have high sand content in the wells up to the seafloor; hence,

there may be little trapping potential. Some are apparent in the southwest (Block 25/3), but these are interpreted to be related to overlying glacial tunnel valleys.

For amplitude anomalies within the clinoforms, these are mostly observed on the eastern side of the study area in the
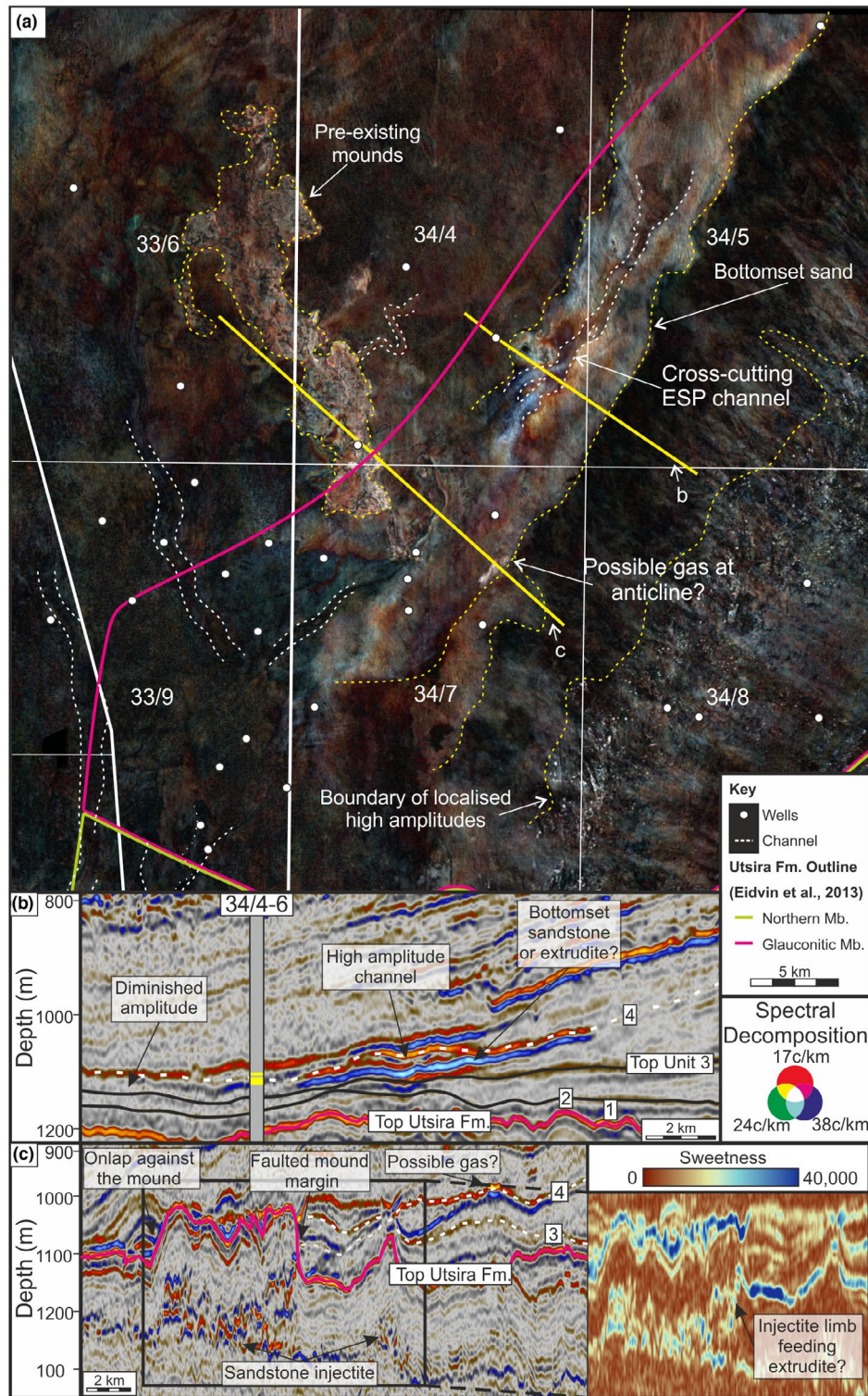
FIGURE 12 Sandstone connectivity between the ESP and NM systems. (a) Frequency decomposition of the Top Unit 4 surface, showing the bottomset sandstones from the NM clinoforms being cross-cut by channels from the ESP, promoting connectivity. (b) Seismic dip section to show the bottomset sandstone in Unit 4, being cross-cut by the possibly sand-filled channel from the ESP. (c) Seismic dip section highlighting the interaction of the sandstone with the mounds (possibly faulted margins) and sand injectite limb. Inset shows the sweetness of Unit 4 sandstone which is possibly sourced from the underlying injectite. Sweetness colour bar from Crameri (2021). Location of 'a' shown in Figure 5

NM clinoforms (red features in Figure 13a). High variance features in the southeast are outlined in Figure 13c and coincide with the channel-lobe complexes (Figures 8 and 13a). High

minimum-amplitude anomalies are positioned within these features (red shading in Figure 13c). These could be shallow gas pockets accumulated in channel sandstones. In the central
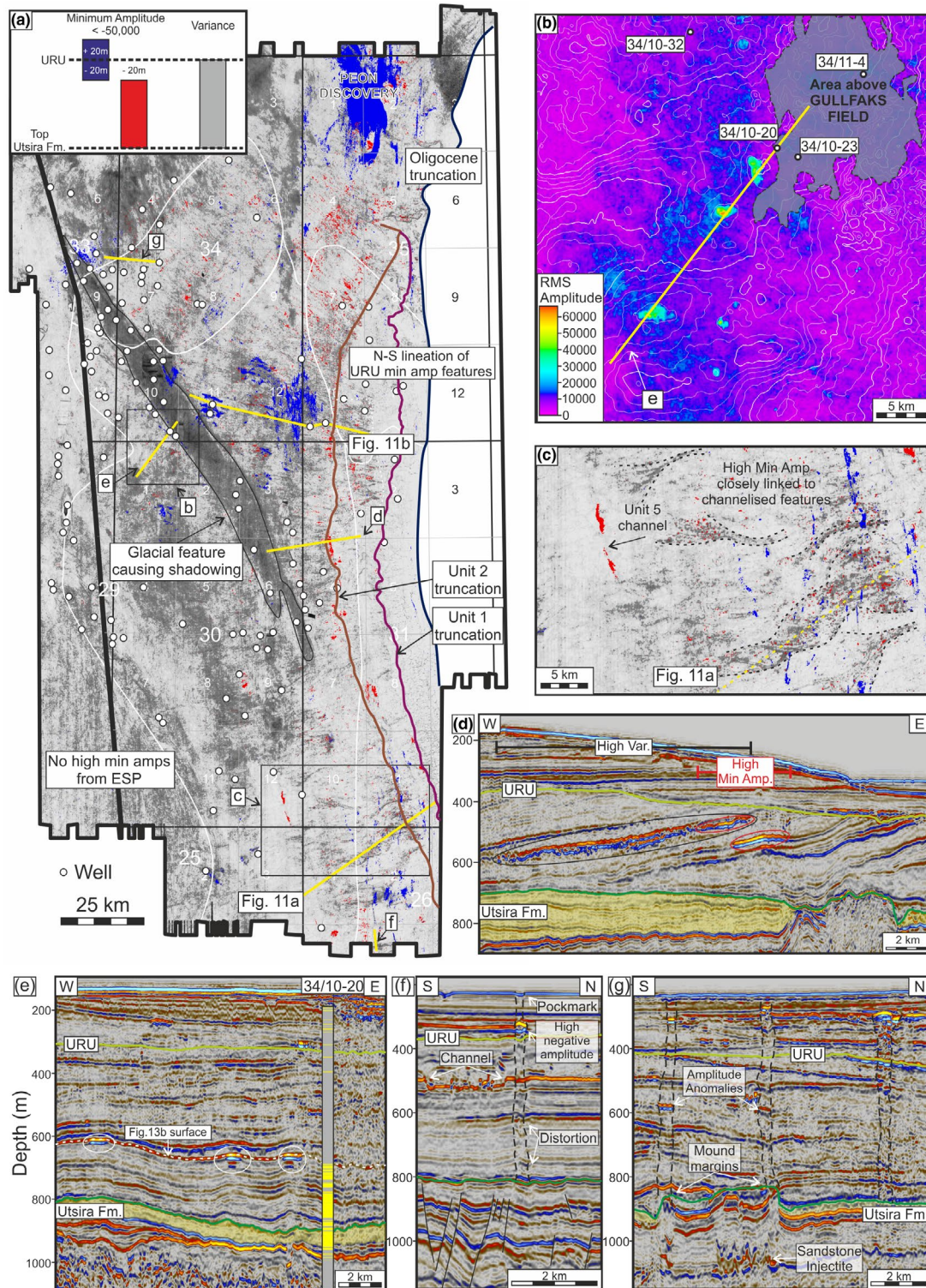
FIGURE 13 Seismic indicators for shallow gas and its migration. (a) Interval variance extraction for the full overburden (URU to Top Utsira Fm.), overlain by minimum amplitude extractions for both the URU (±20 m) and URU (−20 m) to Top Utsira Fm. (b) RMS amplitude map of a surface in the studied interval with depth contours (white), highlighting the possible gas features (high amplitudes) at the crests of anticlines. (c) Zoomed in part of 'a', highlighting the high minimum amplitudes (red) confined to slope channels and the high minimum amplitudes at the URU (blue) that follow the trend of the clinoform truncations from the URU. (d) Seismic dip section to show the seismic character of the high variance and minimum amplitude anomalies within the clinoforms in 'a'; (e) Seismic dip-section of the gas-filled anticlines at the top of the sand from 'b'. (f and g) Seismic cross-sections of seismic chimneys observed within the study area. Neg. Amp., Negative amplitude; Var., Variance

NM clinoforms (Block 31/4), some channel-lobe complexes have anomalously high amplitudes along the whole clinoform (Figure 13d) and exceed the amplitude threshold for a gas indicator on the map in Figure 13a ($<-50{,}000$ amplitude) at their up-dip pinch-out. It is possible that either gas is present and trapped at the URU or tuning from reflector convergence is responsible. High negative amplitudes are also observed on the clinoform below (Figure 13d). The position on an anticline crest suggests it could represent a structurally trapped gas accumulation. In the central and northern NM clinoforms (Quadrant 34 & 35), high negative amplitude anomalies that trend basinward are found in clinothems in distinct clusters coinciding with high variance areas (Figure 13a). These elongated features are chaotic and focused in the slope channels. They may represent gas within sandy channels or be a result of thin-bed tuning. The cross-cutting of the identified channels would result in variable thicknesses, increasing the likelihood of tuning (Figures 7 and 8c,d). On the western side of the basin in the ESP clinoforms, there is a series of anticlines (Blocks 34/10 & 30/1), with high minimum-amplitude crests, trending northeast–southwest, less than 2 km from the margin of the underlying Gullfaks field (Figure 13a,b,e). Well NO 34/10-20 shows that the anomalies sit at the interface between sandstones and overlying mudstones, which supports an interpretation of likely gas pockets, as it became trapped by lower permeability rocks.

6 | DISCUSSION

Various elements of the seal and overburden have been identified and characterised to assess the potential for fluid migration from the Utsira Fm., including: the geometry of the sealing stratigraphy (Figure 5), regional sandstone presence (Figures 6–9) and the vertical connectivity of the reservoir with overlying sandstones (Figures 10 and 11). Here, the results are classified according to regional CO_2 CC. A matrix is presented for classification, which is the first of its kind for regional CO_2 storage assessment, and the region is mapped accordingly (Figures 14 and 15). The evidence for shallow gas and palaeo-migration (Figure 13) is used to support the CC assessment. A fundamental consideration to this assessment is the uncertainties of the approach, which are outlined in Section 6.2. Finally, the importance of this work looking towards a future of upscaled CO_2 storage across the North Sea is discussed.

6.1 | Regional CO_2 CC

6.1.1 | CC framework

The seal for a CO_2 storage reservoir is assessed on a regional scale in the same way as a hydrocarbon reservoir seal, by

mapping components of individual elements that could compromise containment. The elements analysed in this study are as follows: (a) seal geometry; (b) sandstone presence and (c) sandstone connectivity. Each element is scored relatively to the others, as they present variable contributions to containment. For example, sandstone presence is considered to compromise containment more than seal geometry because it represents a possible CO_2 migration path, rather than a juxtaposition that presents a chance for a migration path to be in contact with the reservoir. Components within each element are also assigned relative scoring according to their contribution to containment, for example, 'proven', 'probable' and 'possible' sandstones are assigned progressively lower scores. The two-tiered matrix allows the individual components' scores to range between -8 and $+7$ (Figure 14a). The end values are arbitrary numbers, but are relative, dependent on the number of elements analysed, and the perceived containment contribution by the interpreter.

A CC value of 0 is neutral and is assigned when there is either no data or the feature does not affect containment. A positive value (1 to 8) is assigned where there are features that increase the CC, for example, a proven mudstone seal from wells. A negative value (-1 to -8) is assigned where there are features that decrease the CC, for example, connected overburden sandstones (Figure 14). The features are then mapped to show the spatial distribution of CC of the overburden according to that element (Figure 15a). Each of the element maps were cropped at the border of the Utsira Fm. as focus is on reservoir containment, as opposed to the possible extent of potential fluid migration. The CC scores for the components in a given area are finally summed to provide a total CC score (Schematic, Figure 14b; 'Summary CC Map', Figure 15b), which incorporates all elements for a regional overview.

Seal geometry alone cannot compromise containment without the presence of a seal bypass system (e.g. connected sandstone) and therefore it has a low contribution towards CC. Dipping stratigraphy reduces the CC (CC $= -3$) compared to parallel-to-reservoir seal stratigraphy (CC $= 0$). This is due to the increased probability of an overburden migration path being in contact with the reservoir, along with the provision of a potential up-dip migration route. The spatial distribution of CC as a result of variability in seal geometry is mapped in Figure 15a.

For sandstone presence, CC is dependent upon two factors: (a) the stratigraphic position of the sandstones in relation to the Utsira Fm. and (b) the evidence for sandstone. The position of sandstones relative to the Utsira Fm. is important because those closest to the reservoir present the greatest threat to containment. Subdividing the sandstones according to their units does not indicate proximity to the reservoir due to the highly variable unit thicknesses. As such, for CC assessment, sandstones are split into the Seal and Overburden Intervals (Figure 14).
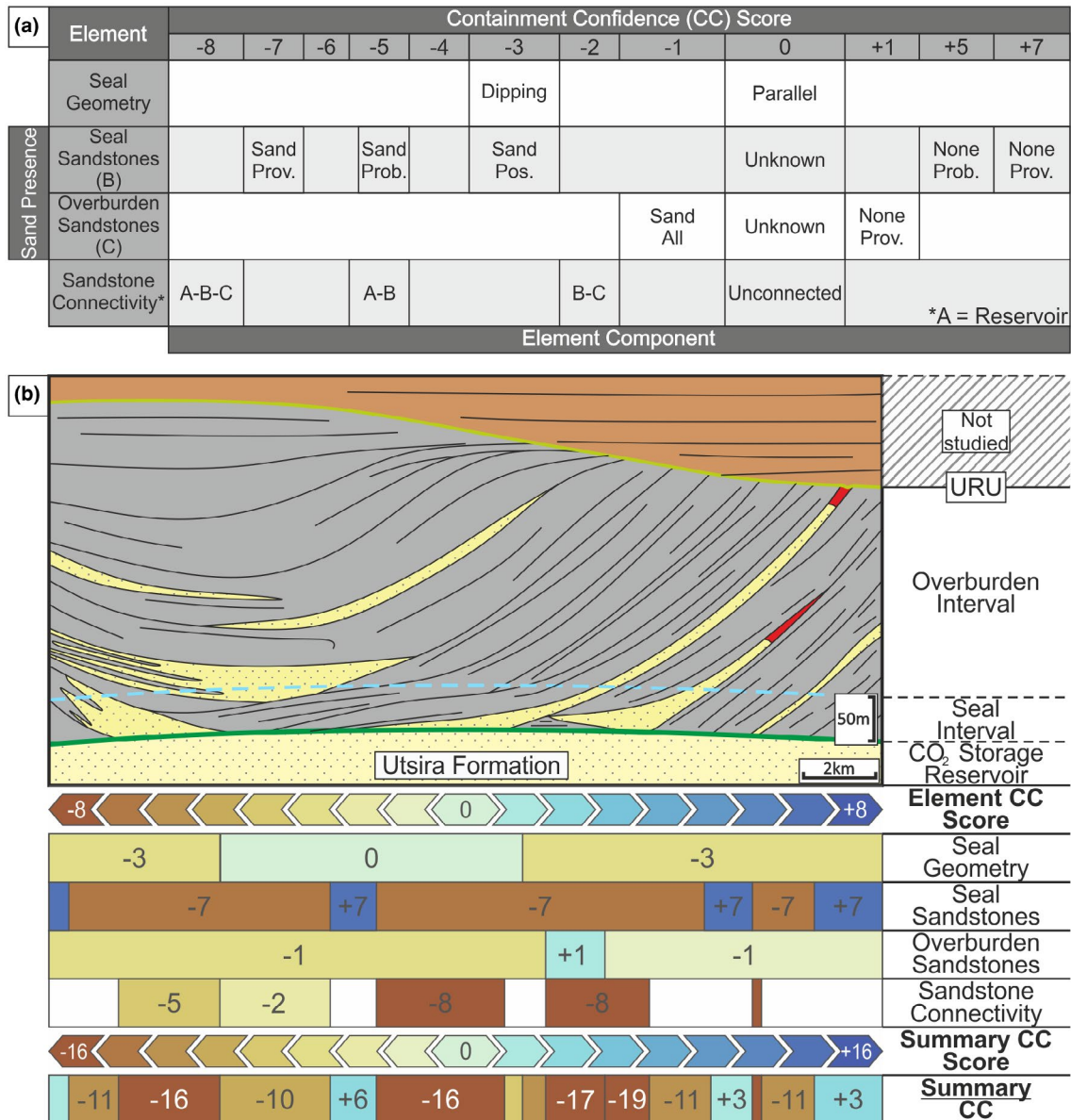
FIGURE 14 Containment confidence (CC) matrix. (a) Containment confidence matrix with relative scoring for each of the seal and overburden elements assessed. Zero is assigned as 'neutral' confidence and is assigned where there are no data available. Negative values are assigned when a feature decreases confidence, and positive values are assigned when a feature increases confidence of containment. prov.= proven, prob.= probable, pos.= possible, referring to the sandstone presence scheme (Figure 7), and also applied to mudstones. (b) Schematic section of seal bypass concepts (from Figure 2b) with the CC matrix applied for each element, including a summary CC score. Sandstones in the conceptual Seal Interval here are assumed to be 'proven'. Colour bar from Crameri (2021)

For sandstone evidence, CC is assigned according to how the sandstones were classified and mapped, regarding their data source (Figure 7). In the Seal Interval, 'proven' sandstones (from well data; CC = −7) reduce CC more than 'probable' (from seismic extrapolation from well data; CC = −5) and 'possible' sandstones (from seismic only; CC = −3). Areas with 'proven' and 'probable' mudstones (through extrapolation using seismic data) are considered to increase the CC and are assigned positive values to mirror proven sandstones (proven mudstone CC = +7; probable mudstone = +5). There is no seismic geomorphology identified in the studied interval that is indicative of mudstone, thus there is not a 'possible' mudstone CC. Possible mudstone CC may be used for deeper CO$_2$ storage targets in the North Sea, where the polygonal faulting could be an indicator for mudstone (e.g. Cartwright, 2011). Where there is sparse well coverage, and no seismic geomorphology that could indicate sandstone presence, the lithology is unknown and CC is considered unchanged (CC = 0). For the Overburden Interval, presence of sandstone alone is not considered to greatly compromise CC, unless there is connectivity. Therefore, a CC value of −1 is assigned if there is any evidence of sandstones,
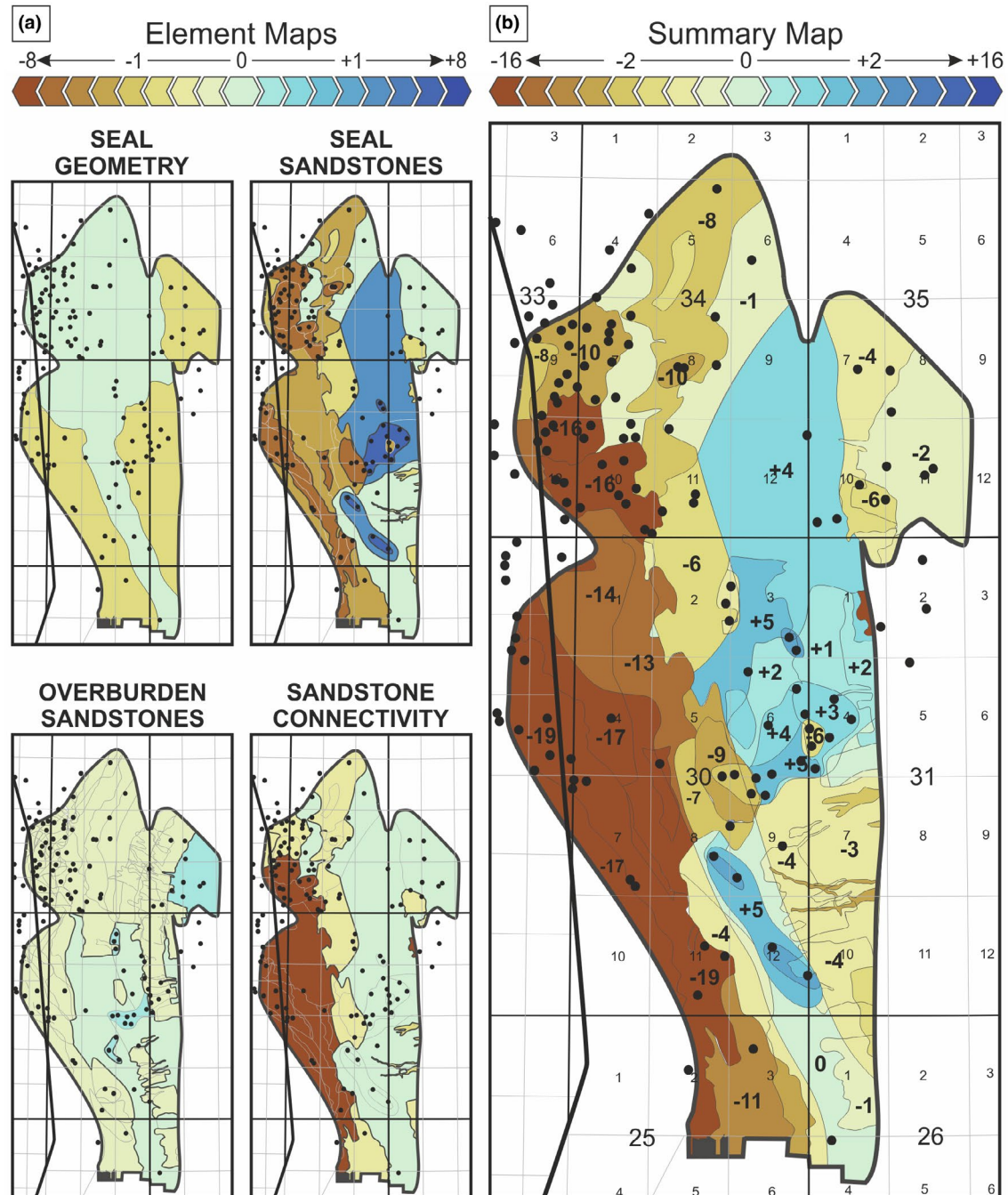
FIGURE 15 Utsira Fm. containment confidence (CC) maps. (a) Individual element maps of the applied CC matrix scheme (Figure 14a). Concept demonstrated in Figure 14b. Grey lines outline individual sandstone bodies identified (Figure 7). (b) Summary CC map of the Utsira Fm., which is the sum of the individual element maps. The map shows the area with the least CC (brown) is towards the west (TS and ESP) and area with the most CC (blue) is in the central and north-eastern parts of the Utsira Fm. Colour bar from Crameri (2021)

+1 if there is a full mudstone succession and 0 where there is no evidence of either (Figures 14 and 15).

This work has shown that there is an inherent difference in sandstone presence between the western ESP and eastern NM prograding systems, as a result of their nonglacial and glacial heritage respectively (Eidvin et al., 2013; Løseth et al., 2020; Ottesen et al., 2014). Although well data from the NM system suggests the shelf is dominated by mudstones, wells in

Blocks 30/6 & 31/4 that penetrate these features contain thin sandstones (Figures 6a,b and 8b,d). This and the shallow gas indicators at the clinoform truncations suggest that despite the glacial origin, sandstones are present within these features that could facilitate CO_2 migration up-dip (Figure 13). Given the features' glacial origin, their general sandstone abundance is likely to be low (Kurjanski et al., 2020) and the sandstone quality is likely to be poorer in terms of porosity

and permeability than the channel and lobe features from the ESP. As such, it could be suggested that their sealing ability is greater than proposed here. Nonetheless, due to data limitations, and that this work is concerned with presence of migration routes rather than quality, a conservative approach was taken, and the features were assigned the same relative scoring as the ESP sandstones.

For the third element, connectivity between the Utsira Fm. (A), sandstones in the 'Seal Interval' (B) and sandstones in the 'Overburden Interval' (C) are assessed. Sandstone connection between 'A', 'B' and 'C' are considered to greatly reduce CC (CC = −8), as it implies full connectivity through the overburden and thus a complete migration route. Connectivity between 'A' and 'B' reduces CC (CC = −5), but not as substantially because secondary migration is inhibited. Connectivity between 'B' and 'C' implies connectivity through the overburden but no connection to the reservoir. This scenario also reduces confidence because sub-seismic features that allow migration through 'B' cannot be ruled out (CC = −2). Where sandstones are disconnected, CC is unchanged with a value of zero. The CC score is applied to the lowermost, nonreservoir sandstone (e.g. bottomset sands in the sealing interval) and not to the whole migration path because that is the root of the connection.

It should be noted that the scheme is applied subjectively and is specifically designed to incorporate the elements deemed important to sealing in this study area. The scheme could be applied to other areas and manipulated to incorporate additional elements, for example, faults or mudstone integrity. In addition, the scheme does not address storage capacity, or does it consider the amount of CO_2 to be injected into the area. As such, it should not be viewed as a chance of success, or a measure of the relative amount of CO_2 that could be stored. The purpose is to qualitatively highlight better or worse regions for containment of CO_2, as a result of seal bypass, which could be the focus of future studies.

6.1.2 | CC regional summary

As shown by the Summary Map (Figure 15b), the area with the highest CC is in the central and northern part of the study area, in Blocks 30/3, & 34/12, where the range in total CC score is +2 to +5. Here, there are flat-lying reflections overlying the Utsira Fm. For >50 m (seal geometry CC = 0), and mudstone is either 'proven' or 'probable' (seal sandstone presence CC = +5 or +7) in the Seal Interval. Sandstones were encountered in the Seal Interval in wells NO 31/4-1 and 31/4-7 but are noncorrelatable, isolated and unconnected (sand connectivity CC = 0). Sandstones are 'possible' in the Overburden Interval (overburden sandstone presence CC = −1), but they are unconnected (sand connectivity CC = 0). Interpretation of shallow gas (and its migration

from deeper sources where applicable) is used to support the findings from the summary CC map. The central and northern area presents little evidence of gas, with the exception of one large high negative amplitude feature above the URU (Figures 11b and 13). The feature does not follow the trend of the URU-clinoform truncations and there are no clear vertical migration structures, hence if the feature is interpreted to be gas, it is likely in-place with biogenic origin. Considering the seal aspect of the CO_2 storage play, this area would therefore be most suitable for injection.

The area with lowest total CC score that could present the greatest risk of migration upon injection is the west of the study area (ESP & Tampen Spur region), with total CC ranging −4 to −19 (Figure 15b). The range is high because there is substantial variability in the seal elements spatially. Stratigraphy within 50 m of Top Utsira Fm. is flat lying in the northwest (Tampen Spur) and dipping in the southwest, resulting in containment scores of 0 and −3 respectively. 'Proven', 'probable' and 'possible' sandstones are present in both the Seal and Overburden Intervals (sandstone presence CC = −4 to −10). Seal Interval sandstones are in connection or close connection (seismically nonresolvable mudstone barrier) with the Utsira Fm. and subsequently connected to overburden sandstones that provide up-dip secondary migration paths (sandstone connectivity CC = −8). In some areas, there are Seal Interval sandstones connected to Overburden Interval sandstones, but disconnected from the Utsira Fm., and therefore primary migration is inhibited (sandstone connectivity CC = −2). In the northwest, gas appears to have accumulated within anticlinal structures ca. 180 m above the Utsira Fm., 3 km west of the Gullfaks field (Figure 13), which suggests that it may have migrated into place. This is evidence to support the low containment score due to overburden sandstone presence/connectivity. Considering the seal aspect of the CO_2 storage play, this area would therefore be least suitable for injection.

The area to the southeast (Blocks 31/7 & 31/10) presents total CC scores of −3 to −9. There is dipping seal stratigraphy (seal geometry CC = −3), 'possible' sandstones or unknown lithology in both the Seal and Overburden Intervals (sandstone presence CC = −3 to 0), and connection of the Utsira Fm. to Seal Interval sandstones, promoting primary migration (sandstone connection CC = −5). In the southeast, gassy signatures are observed to follow the trend of the clinoform truncations suggesting that gas migrated up the clinoforms and is trapped at the URU. This also supports the low containment score in the area that reflects likely sandstone connectivity through the overburden (Figure 13). However, as previously stated, these CC scores are conservative, that is, they could be more positive with higher mud content (and lower permeability) than predicted, as a result of the dominant glacial process regime on the NM.

The southwest is another low-scoring area in terms of CC, but does not have any gas highlighted from the analysis, for

which there may be four explanations: (a) gas is dissolved in pore water and not detected in seismic data (e.g. Abrams, 2017), (b) gas signatures are masked from tuning or porosity effects and do not meet the amplitude threshold used in the attribute analysis (Barrett et al., 2017); (c) gas migrated vertically through the abundant sandstones in the clinoforms with little impedance or trapping (through connected sandstones, Figure 15b), and escaped at the seabed, but there are few diagnostic features, such as pockmarks; and (d) there is no shallow gas in the area.

6.2 | Data and interpretation uncertainties

Uncertainty of approaches, results and interpretations are fundamental considerations in the assessment of a CO_2 seal, particularly if the conclusions should direct future focus areas and form the basis of predictions. Here, although the results and interpretations may be as free from subjective considerations as is possible, the conclusions of the study should be treated with caution. Several uncertainties associated with the workflow and data analysis are qualitatively described below.

1. Well distribution. The region with highest abundance of overburden sandstones and the lowest CC is also the area with the highest well density (Tampen Spur, Figure 15b). Moreover, the region with the lowest abundance of overburden sandstones, and highest CC is the area with fewest wells (northeast Utsira Fm. Figure 15b). Therefore, one could argue that sandstone presence relates to the well distribution and direct observation. However, wells in the Tampen Spur region have a series of seismically resolvable sandstones in Units 1–4, which are not observed in any individual well in other areas. Also, sandstone bodies in the Tampen Spur region have a characteristic geometry and high negative amplitude seismic signature, which is not observed in the northeast. It is possible that sandstones do exist in the northeast, but none were observed from seismic attributes (amplitude, sweetness or variance) or the limited well data. Additional data analysis such as seismic inversion may help reduce this uncertainty.

2. Mudstone integrity. The thickness of the mudstone buffer between the Utsira Fm. and the overlying sandstones is shown to be highly variable, where present. Mudstone thickness is a useful indicator of containment, but geotechnical properties of the mudstone are required to understand whether it has the potential to seal CO_2 and are not constrained here. For example, the degree of consolidation and micro-fracturing, and therefore permeability of mudstones at the shallow depths examined (<1,000 m) is unclear, and likely to be variable as a result of the subjected glacial loading and unloading through the Quaternary (Medvedev

et al., 2019; Olsen et al., 2013). Previous work on mudstone integrity for Cenozoic CO_2 storage in the North Sea have focused on deeper CO_2 storage systems (Nooraiepour et al., 2017), or on the mudstones at the Sleipner storage site (e.g. Nicoll, 2012; Verdon et al., 2013). A gas discovery in 2015 (Zulu Øst), in the southern Utsira Fm. (outside of the study area) proved that the Utsira Fm. seal can trap a fluid column in parts (NPD, 2015). However, there is some doubt cast upon thin (below seismic resolution) mudstones for sealing, since CO_2 was found to unexpectedly bypass meter-scale (<7 m) mudstone barriers within the Utsira CO_2 reservoir above the Sleipner field in the first 3 years of injection (Gregersen & Johannessen, 2001; Zweigel et al., 2004). It is unclear whether this was due to the geometry (e.g. pinch-out) or integrity of the mudstone (Zweigel et al., 2004). Characterising mudstone integrity is beyond the scope of this study, but should be carefully considered, especially where mudstones are relatively thin. Further analysis on the mudstones using the dataset could be achieved with a more concentrated focus on the mudstones (as opposed to the sandstones here) and seismic inversion to constrain densities and porosities.

3. Data resolution. Sandstones and mudstones below seismic resolution are encountered in the wells in both interbedded complexes or as individual beds encased in the opposing lithology. Thin beds can both promote connectivity (e.g. sandstone beds observed in the NM clinoform foresets in Units 1–4) or restrict it (e.g. thin mudstone beds in the Tampen Spur region in Units 1–4). For both thin bed types, extensive lateral coverage is needed to influence connectivity; either sandstones need to be present along the entire length of a foreset for secondary migration, or total coverage of a mudstone bed is required over a sandstone to act as a barrier rather than a baffle to flow. However, where pinch-out and erosion are unresolvable, their full lateral extent is unknown, which ultimately restricts understanding of precisely where sandstones are in direct connection or where migration between sands could be buffered. Thin beds can act both positively and negatively towards containment, their potential contribution is acknowledged, but not constrained in the CC matrix. As connectivity could be greater than constrained with the data and confidence could be lower, to be conservative, CC values should be considered as maximum values.

4. Faulting. Faults can present a high risk to containment if they provide a fluid conduit, or may be a useful trapping mechanism if they are sealing (Aydin, 2000). However, no major faults were identified. The polygonal faulted units prevalent in the northern North Sea (e.g. in the Hordaland Group) are deeper than the studied stratigraphic interval. In the Tampen Spur region there are several mounds protruding from the underlying succession of the Utsira Fm. If their margins are faulted (Løseth et al., 2013; Rundberg

& Eidvin, 2016), they could present migration routes into the Seal Interval. Small-scale faults (below seismic resolution) have been hypothesised to be the cause of intra-formation seal breach (metre-scale mudstones) at Sleipner, as a result of post-depositional ice-sheet loading and unloading (Cavanagh & Haszeldine, 2014; Løtveit et al., 2019). Similar small-scale faulting could be present in the study area, but here a minimum seal thickness of 50 m is required and thus they are unlikely to present a major risk to CO_2 containment. High-angle faults that are not imaged in seismic data are possible, but given the structural context are deemed unlikely.

5. Legacy wells. This study does not consider leakage through legacy wells (abandoned exploration and production wells). This is because the effect of legacy wells on leakage is debated, with the effects likely to depend on the age, type of cementation, type of plugging, overpressure and other failure conditions (Ide et al., 2006). In the Central North Sea, 28 of 43 studied decommissioned wells had evidence of leakage of gas into the water column (Böttner et al., 2020). Nevertheless, areas highlighted in this study with the greatest CC have relatively low well density.

6. Gas artefacts. In the absence of AVO studies, seismic inversion and fluid substitution, the interpretation of gas from seismic can only be undertaken in a qualitative manner – that is, gas probability can be assessed, but not the definitive presence or absence of gas. It is possible that the seismic indicators used here to highlight potential gas presence and palaeo-gas migration can be produced by different geological processes, including: (a) velocity pull-downs and acoustic blanking from overlying glacial valleys (Huuse & Kristensen, 2016); (b) pockmarks caused by de-watering (Andresen & Huuse, 2011) and (c) high-amplitude reflections from thin bed tuning or lithological effects (Barrett et al., 2017). Although not used here, well data are highly informative at identifying gas (Buckley & Cottee, 2017).

6.3 | Implications for CO_2 storage site selection

CCS is viewed as a critical part of the solution to reduce global net CO_2 emissions (IEA, 2016, 2017; Stocker, 2014). In order to upscale global operations, identification of suitable CO_2 storage sites is required. The Utsira Fm. has proven CO_2 storage capabilities at the Sleipner Field, where over 17 Mt of CO_2 have been successfully contained (Furre et al., 2017). This study has shown that CC of the seal and overburden is not uniform across the northern Utsira Fm. as a result of potential fluid migration pathways, and this must be considered in future CO_2 storage site selection.

This study shows that the areas with the lowest CC and therefore areas to be avoided for CO_2 injection are on the western side of the Utsira Fm., specifically the Tampen Spur region and around the ESP. In both areas, there are bottom-set sandstones either in connection or close connection (seismically nonresolvable mudstone barrier) to the Utsira Fm. with connected up-dip migration paths, or a full vertical sandstone succession. These areas would be unlikely candidates for CO_2 storage based on the reservoir, as most of the Utsira Fm. in the Tampen Spur region is represented by a thin glauconitic sandstone (Figure 1) (Eidvin et al., 2013). Around the ESP, the Utsira Fm. is too shallow for storage as CO_2 would leave the supercritical phase at ca. 800 m depth (Halland et al., 2011; White et al., 2003). Even though this region is not ideal for injection itself, given its shallow depth, it is possible that CO_2 injected into other areas of Utsira Fm. would preferentially migrate towards it and thus present high potential for loss from the reservoir. As such, it is recommended that future CO_2 plume simulations of the reservoir consider and incorporate the seal and overburden CC map provided here (Figure 15). Areas of generally high CC, but with localised low CC (e.g. Block 30/6, where CC is positive except for a small area where CC = −6 in Figure 15b), should be similarly considered. Although they may exhibit suitable CO_2 containment conditions, as the CO_2 plume expands within the reservoir, it could enter a region of lower CC. Furthermore, simulations through a high-resolution static overburden model that incorporates the elements constrained here would help to understand the timescale of potential migration to the seabed.

The region of highest CC is in the central and northeast study area, particularly in Blocks 30/3, 31/1, 34/12 and most of 30/6 and 31/4. In these areas, the only sandstones identified in the overburden are unconnected to the reservoir by mudstones in the Seal Interval. Higher-resolution mapping of seal elements in this area should be undertaken prior to site selection to fully characterise mudstone barriers and thin sandstone migration paths, and seal integrity analysis is required. However, this region coincides with a thick part of the northern Utsira Fm. (depocentre with ca. 200 m thickness) in Blocks 30/2, 30/3, 30/5 & 30/6 (Figures 1 and 15b), and thus this area may be optimal for storage with both preferential reservoir and seal conditions.

7 | CONCLUSIONS

The Utsira Fm. in the northern North Sea is a potentially promising reservoir target for upscaled CO_2 storage, but a minimum requirement is that CO_2 can be contained via a low permeability, laterally extensive seal. Through regional identification, assessment and mapping of the key elements that could facilitate seal bypass (seal geometry, sandstone

presence and sandstone connectivity), a CO_2 containment confidence (CC) matrix has been developed. This has been applied to the Utsira Fm. and can be used to inform CO_2 storage site selection.

For seal geometry, the Seal Interval (<50 m above the reservoir) comprises dipping stratigraphy (clinoform foresets) that juxtapose multiple clinothems against the reservoir, increasing the potential for up-dip migration paths in the south of the study area. Conversely, in the central and northwest, stratigraphy is approximately parallel to the reservoir, which restricts vertical migration. Sandstones were mapped using a 'proven', 'probable' and 'possible' sandstone presence scheme and connectivity between them was assessed. In the bottomsets of the main prograding clinoform units (Units 1–4), thick sandstones were identified from wells in the Tampen Spur region, around the ESP and in the central part of the basin (Blocks 30/5). Only the latter region had a resolvable, continuous mudstone separating the sandstones from the reservoir. In the Tampen Spur region, the intervening mudstones in the Seal Interval have variable thickness and in some areas sandstones are directly connected to the reservoir, implying primary migration would be possible. The Overburden Interval (>50 m above the Utsira Fm.) comprises a thick mudstone succession, which could restrict vertical, secondary migration to the URU. However, slope channels have been identified on the ESP clinoform foresets that extend down-dip to the Tampen Spur region and could provide up-dip migration paths towards the ESP. Around the ESP itself, there are intervals with 'proven' sandstone from the Top Utsira Fm. to the URU. Further channel-lobe complexes were identified along the entire Norwegian Margin clinoform system. Lithologies within these channel-lobe complexes are poorly sampled by existing wells, thus their lithology distribution is uncertain, but they appear to be mudstone dominated with some sandstones. If sandstones are present, they could provide up-dip migration paths through the overburden. However, apart from the south-eastern side of the basin, these are separated from the Utsira Fm. by >50 m of mudstone. Shallow gas evidence in the seismic data is assessed to support the seal elements analysis, as it may indicate previous (and potential for future) fluid migration; for example, gas appears to be trapped at the URU-clinoform truncations in the southeast and may have migrated from below.

Each element was assigned a CC score, and these were summed to map overall CC of the Utsira Fm. The areas with the lowest CC, and therefore recommended to be avoided for CO_2 site selection, are on the western side of the Utsira Fm. around the ESP and the Tampen Spur region. In both areas, there are connected seal and overburden sandstones, with migration possible, either vertically at the ESP through the full sandstone succession present here, or up-dip through the multiple, cross-cutting, sandy submarine channel systems. Although the region is not ideal for injection itself, the reservoir in this area is relatively shallow and injected CO_2 from elsewhere could preferentially migrate towards it. Thus, the CC map provided could be used to inform future CO_2 plume simulation analyses. The areas with the highest CC and therefore most suitable for CO_2 storage are the central and northern parts of the Utsira Fm. These are high scoring areas due to the flat-lying seal geometry and mudstone-dominated Seal Interval. Uncertainties in the analysis are considered and exist as a result of data distribution, data resolution and unknown influences of sub-seismic faults, legacy wells and mudstone integrity. For the areas highlighted to be suitable for CO_2 storage, further localised research on the seal with focus on mudstone integrity is required, as well as a full reservoir appraisal.

CONFLICT OF INTEREST
The authors have declared no conflicts of interest for this article.

PEER REVIEW
The peer review history for this article is available at https://publons.com/publon/10.1111/bre.12545.

DATA AVAILABILITY STATEMENT
The data that support the findings of this study are available from CGG. Restrictions apply to the availability of these data, which were used under license for this study. Data are available from the authors with the permission of CGG.

ORCID

Christopher Lloyd https://orcid.org/0000-0001-5011-1284

Mads Huuse https://orcid.org/0000-0002-1766-4343

Bonita J. Barrett https://orcid.org/0000-0002-3274-822X

Andrew M. W. Newton https://orcid.org/0000-0002-0089-525X

REFERENCES

Abrams, M. A. (2017). Evaluation of near-surface gases in marine sediments to assess subsurface petroleum gas generation and entrapment. *Geosciences*, *7*, 35. https://doi.org/10.3390/geosciences7020035

Andresen, K. J., & Huuse, M. (2011). 'Bulls-eye' pockmarks and polygonal faulting in the Lower Congo Basin: Relative timing and implications for fluid expulsion during shallow burial. *Marine Geology*, *279*, 111–127. https://doi.org/10.1016/j.margeo.2010.10.016

Arntsen, B., Wensaas, L., Løseth, H., & Hermanrud, C. (2007). Seismic modeling of gas chimneys. *Geophysics*, *72*, 251–259. https://doi.org/10.1190/1.2749570

Aydin, A. (2000). Fractures, faults, and hydrocarbon entrapment, migration and flow. *Marine and Petroleum Geology*, *17*, 797–814. https://doi.org/10.1016/S0264-8172(00)00020-9

Bacon, M., Simm, R., & Redshaw, T. (2003). Interpreting seismic amplitudes. In *3-D Seismic Interpretation* (pp. 120–154). Cambridge: Cambridge University Press. https://doi.org/10.1017/CBO9780511802416.006

Barrett, B. J., Huws, D. G., Booth, A. D., Wergeland, Ø., & Green, J. M. (2017). Tuning, interference and false shallow gas signatures in geohazard interpretations: Beyond the 'λ/4' rule. *Near Surface Geophysics*, *15*, 359–366. https://doi.org/10.3997/1873-0604.2017023

Batchelor, C. L., Ottesen, D., & Dowdeswell, J. A. (2017). Quaternary evolution of the northern North Sea margin through glacigenic debris-flow and contourite deposition. *Journal of Quaternary Science*, *32*, 416–426. https://doi.org/10.1002/jqs.2934

Bøe, R., Magnus, C., Osmundsen, P. T., & Rindstad, B. I. (2002). CO_2 point sources and subsurface storage capacities for CO_2 in aquifers in Norway, NGU Report 2002.

Böttner, C., Haeckel, M., Schmidt, M., Berndt, C., Vielstädte, L., Kutsch, J. A., Karstens, J., & Weiß, T. (2020). Greenhouse gas emissions from marine decommissioned hydrocarbon wells: Leakage detection, monitoring and mitigation strategies. *International Journal of Greenhouse Gas Control*, *100*, 103–119. https://doi.org/10.1016/j.ijggc.2020.103119

Brown, C. S., Newton, A. M., Huuse, M., & Buckley, F. (2017). Iceberg scours, pits, and pockmarks in the North Falkland Basin. *Marine Geology*, *386*, 140–152. https://doi.org/10.1016/j.margeo.2017.03.001

Buckley, F. A., & Cottee, L. (2017). A petrophysical approach to the investigation of shallow marine geology. *Near Surface Geophysics*, *15*, 367–385. https://doi.org/10.3997/1873-0604.2017031

Bugge, T., Tveiten, B., & Bäckström, S. (2001). The depositional history of the Cretaceous in the northeastern North Sea. *Norwegian Petroleum Society Special Publications*, *10*, 279–291.

Cartwright, J. (2011). Diagenetically induced shear failure of fine-grained sediments and the development of polygonal fault systems. *Marine and Petroleum Geology*, *28*, 1593–1610. https://doi.org/10.1016/j.marpetgeo.2011.06.004

Cartwright, J., Huuse, M., & Aplin, A. (2007). Seal bypass systems. *AAPG Bulletin*, *91*, 1141–1166. https://doi.org/10.1306/04090705181

Cavanagh, A. J., & Haszeldine, R. S. (2014). The Sleipner storage site: Capillary flow modeling of a layered CO_2 plume requires fractured shale barriers within the Utsira Formation. *International Journal of Greenhouse Gas Control*, *21*, 101–112. https://doi.org/10.1016/j.ijggc.2013.11.017

Chadwick, A., Arts, R., Bernstone, C., May, F., Thibeau, S., & Zweigel, P. (Eds.) (2008). *Best practice for the storage of CO2 in saline aquifers, Observations and guidelines from the SACS and CO2STORE projects*. BGS Occasional Publication No. 14. BGS.

Chadwick, R. A., Zweigel, P., Gregersen, U., Kirby, G. A., Holloway, S., & Johannessen, P. N. (2004). Geological reservoir characterization of a CO_2 storage site: The Utsira Sand, Sleipner, northern North Sea. *Energy*, *29*, 1371–1381. https://doi.org/10.1016/j.energy.2004.03.071

Chand, S., Thorsnes, T., Rise, L., Brunstad, H., Stoddart, D., Bøe, R., Lågstad, P., & Svolsbru, T. (2012). Multiple episodes of fluid flow in the SW Barents Sea (Loppa High) evidenced by gas flares, pockmarks and gas hydrate accumulation. *Earth and Planetary Science Letters*, *331*, 305–314. https://doi.org/10.1016/j.epsl.2012.03.021

Constable, S. (2010). Ten years of marine CSEM for hydrocarbon exploration. *Geophysics*, *75*, 75A67–75A81. https://doi.org/10.1190/1.3483451

Coward, M. P., Dewey, J. F., Hempton, M., & Holroyd, J. (2003). Tectonic evolution. In D. Evans, C. Graham, A. Armour, & P. Bathurst (Eds.), *The Millennium Atlas: petroleum geology of the central and northern North Sea* (pp. 17–33). London: The Geological Society of London.

Crameri, F. (2021). Scientific colour maps: Perceptually uniform and colour-blind friendly. *Zenodo*, https://doi.org/10.5281/zenodo.1243862

Dalland, A., Worsley, D., & Ofstad, K. (Eds.) (1988). A lithostratigraphic scheme for the mesozoic and cenozoic and succession offshore mid-and northern norway. *Oljedirektoratet*.

Daynac, N., Lacaze, S., & Pauget, F. (2016). Interpretation of complex faulted deposits in the North Sea using the relative geological time model. *First Break*, *34*, 55–62. https://doi.org/10.3997/1365-2397.2016006

De Schepper, S., & Mangerud, G. (2017). Age and palaeoenvironment of the Utsira Formation in the northern North Sea based on marine palynology. *Norwegian Journal of Geology*, *97*, 305–326.

Eidvin, T., Riis, F., & Rasmussen, E. S. (2014). Oligocene to Lower Pliocene deposits of the Norwegian continental shelf, Norwegian Sea, Svalbard, Denmark and their relation to the uplift of Fennoscandia: A synthesis. *Marine and Petroleum Geology*, *56*, 184–221. https://doi.org/10.1016/j.marpetgeo.2014.04.006

Eidvin, T., Riis, F., Rasmussen, E. S., & Rundberg, Y. (2013). Investigation of Oligocene to Lower Pliocene deposits in the Nordic offshore area and onshore Denmark. *NPD Bulletin*, *10*, 62.

Eidvin, T., & Rundberg, Y. (2001). Late Cainozoic stratigraphy of the Tampen area (Snorre and Visund fields) in the northern North Sea, with emphasis on the chronology of early Neogene sands. *Norwegian Journal of Geology/Norsk Geologisk Forening*, *81*, 119–160.

EMODnet Bathymetry Consortium. (2018). EMODnet Digital Bathymetry (DTM 2018). EMODnet Bathymetry Consortium.

European-Commission. (2018). A Clean Planet for all: A European long-term strategic vision for a prosperous, modern, competitive

and climate neutral economy. In *In-depth analysis in support of the commission communication*. Brussels: European Commission.

Færseth, R. B. (1996). Interaction of Permo-Triassic and Jurassic extensional fault-blocks during the development of the northern North Sea. *Journal of the Geological Society*, *153*, 931–944. https://doi.org/10.1144/gsjgs.153.6.0931

Floodgate, G. D., & Judd, A. G. (1992). The origins of shallow gas. *Continental Shelf Research*, *12*, 1145–1156. https://doi.org/10.1016/0278-4343(92)90075-U

Furre, A. K., Eiken, O., Alnes, H., Vevatne, J. N., & Kiær, A. F. (2017). 20 years of monitoring CO_2-injection at Sleipner. *Energy Procedia*, *114*, 3916–3926. https://doi.org/10.1016/j.egypro.2017.03.1523

Galloway, W. E. (2002). Paleogeographic setting and depositional architecture of a sand-dominated shelf depositional system, Miocene Utsira Formation, North Sea Basin. *Journal of Sedimentary Research*, *72*, 476–490. https://doi.org/10.1306/110801720476

Gasda, S., Wangen, M., Bjørnara, T., & Elenius, M. (2017). Investigation of caprock integrity due to pressure build-up during high-volume injection into the Utsira formation. *Energy Procedia*, *114*, 3157–3166. https://doi.org/10.1016/j.egypro.2017.03.1444

GCCSI. (2020). Global status of CCS: 2020. www.globalccsinstitute.com/resources/global-status-report/

Gregersen, U., & Johannessen, P. N. (2001). The Neogene Utsira sand and its seal in the Viking Graben area, North Sea saline aquifer CO_2 storage (SACS) project, phase 2 task 1.7 geology. *Geological Survey of Denmark and Greenland Report*, *100*, 1–2.

Gregersen, U., & Johannessen, P. N. (2007). Distribution of the Neogene Utsira Sand and the succeeding deposits in the Viking Graben area, North Sea. *Marine and Petroleum Geology*, *24*, 591–606. https://doi.org/10.1016/j.marpetgeo.2007.04.006

Halland, E., Johansen, W., & Riis, F. (2011). *CO_2 Storage Atlas, Norwegian North Sea*. Publication of the Norwegian Petroleum Directorate.

Han, C. (2019). Spectral decomposition AVO attributes for identifying potential hydrocarbon-related frequency anomalies. *First Break*, *37*, 89–97. https://doi.org/10.3997/1365-2397.n0027

Hayes, P., Twigger, L., Ubik, K., Latter, T., Purcell, C., Xiao, B., & Ratcliffe, A. (2018). Increasing resolution in the North Sea. *First Break*, *36*, 105–111. https://doi.org/10.3997/1365-2397.n0141

Hepple, R. P., & Benson, S. M. (2005). Geologic storage of carbon dioxide as a climate change mitigation strategy: Performance requirements and the implications of surface seepage. *Environmental Geology*, *47*, 576–585. https://doi.org/10.1007/s00254-004-1181-2

Höller, S., & Viebahn, P. (2011). Assessment of CO_2 storage capacity in geological formations of Germany and Northern Europe. *Energy Procedia*, *4*, 4897–4904. https://doi.org/10.1016/j.egypro.2011.02.458

Holloway, S. (Ed.) (1996). *The underground disposal of carbon dioxide, Final report of Joule 2, Project No. CT92-0031* (p. 355). British Geological Survey.

Hovland, M., & Judd, A. G. (1988). *Seabed pockmarks and seepages: Impact on geology, biology and the marine environment*. Graham & Trotman.

Hovland, M., Judd, A. G., & King, L. H. (1984). Characteristic features of pockmarks on the North Sea Floor and Scotian Shelf. *Sedimentology*, *31*, 471–480.

Huuse, M., & Kristensen, T. B. (2016). Pleistocene tunnel valleys in the North Sea Basin. *Geological Society, London, Memoirs*, *46*, 207–208.

Ide, S. T., Friedmann, S. J., & Herzog, H. J. (2006). CO_2 leakage through existing wells: Current technology and regulations. In *8th International Conference on Greenhouse Gas Control Technologies* (Vol. *1*, pp. 19–33).

IEA. (2016). 20 years of carbon capture and storage: Accelerating future deployment. www.iea.org/publications

IEA. (2017). Energy Technology Perspectives in 2017.

Isaksen, D.,& Tonstad, K. (1989). *A revised Cretaceous and Tertiary lithostratigraphic nomenclature for the Norwegian North Sea*. Norwegian Petroleum Directorate.

Jordt, H., Faleide, J. I., Bjørlykke, K., & Ibrahim, M. T. (1995). Cenozoic sequence stratigraphy of the central and northern North Sea Basin: Tectonic development, sediment distribution and provenance areas. *Marine and Petroleum Geology*, *12*, 845–879.

Judd, A. G., & Hovland, M. (1992). The evidence of shallow gas in marine sediments. *Continental Shelf Research*, *12*, 1081–1095.

Kurjanski, B., Rea, B. R., Spagnolo, M., Cornwell, D. G., Howell, J., & Archer, S. (2020). A conceptual model for glaciogenic reservoirs: From land systems to reservoir architecture. *Marine and Petroleum Geology*, *115*, 104205. https://doi.org/10.1016/j.marpetgeo.2019.104205

Lie, K. A., Nilsen, H. M., Andersen, O., & Møyner, O. (2016). A simulation workflow for large-scale CO_2 storage in the Norwegian North Sea. *Computers & Geosciences*, *20*, 607–622.

Løseth, H., Dowdeswell, J. A., Batchelor, C. L., & Ottesen, D. (2020). 3D sedimentary architecture showing the inception of an Ice Age. *Nature Communications*, *11*, 1–7.

Løseth, H., Gading, M., & Wensaas, L. (2009). Hydrocarbon leakage interpreted on seismic data. *Marine and Petroleum Geology*, *26*, 1304–1319. https://doi.org/10.1016/j.marpetgeo.2008.09.008

Løseth, H., Raulline, B., & Nygård, A. (2013). Late Cenozoic geological evolution of the northern North Sea: Development of a Miocene unconformity reshaped by large-scale Pleistocene sand intrusion. *Journal of the Geological Society*, *170*, 133–145. https://doi.org/10.1144/jgs2011-165

Løseth, H., Rodrigues, N., & Cobbold, P. R. (2012). World's largest extrusive body of sand? *Geology*, *40*, 467–470. https://doi.org/10.1130/G33117.1

Løtveit, I. F., Fjeldskaar, W., & Sydnes, M. (2019). Tilting and flexural stresses in basins due to glaciations—An example from the Barents Sea. *Geosciences*, *9*, 474. https://doi.org/10.3390/geosciences9110474

Martinsen, O. J., Bøen, F., Charnock, M. A., Mangerud, G., & Nøttvedt, A. (1999). Cenozoic development of the Norwegian margin 60–64° N: Sequences and sedimentary response to variable basin physiography and tectonic setting. *Geological Society, London, Petroleum Geology Conference Series*, *5*, 293–304. https://doi.org/10.1144/0050293

Medvedev, S., Hartz, E. H., Schmid, D. W., Zakariassen, E., & Varhaug, P. (2019). Influence of glaciations on North Sea petroleum systems. *Geological Society, London, Special Publications*, *494*, SP494-2018. https://doi.org/10.1144/SP494-2018-183

Myung, L., & William, D. (2001). Amplitude blanking related to the pore-filling of gas hydrate in sediments. *Marine Geophysical Researches*, *22*, 101–109.

Nicoll, G. D. (2012). *Evaluation of the Nordland Group overburden as an effective seal for the Sleipner CO_2 storage site (offshore Norway) using analytical and stochastic modelling techniques*. University of Edinburgh. PhD Thesis.

Nooraiepour, M., Haile, B. G., & Hellevang, H. (2017). Compaction and mechanical strength of Middle Miocene mudstones in the Norwegian North Sea–The major seal for the Skade CO_2 storage

reservoir. *International Journal of Greenhouse Gas Control*, *67*, 49–59. https://doi.org/10.1016/j.ijggc.2017.10.016

Nøttvedt, A., Gabrielsen, R. H., & Steel, R. J. (1995). Tectonostratigraphy and sedimentary architecture of rift basins, with reference to the northern North Sea. *Marine and Petroleum Geology*, *12*, 881–901. https://doi.org/10.1016/0264-8172(95)98853-W

NPD. (2015). Lundin Norway AS, operator of production license 674 BS, is finalizing drilling of exploration well 26 / 10–1. Norwegian Petroleum Directorate. https://www.npd.no/fakta/nyheter/Resultat-av-leteboring/2015/2610-1/

Olsen, L., Sveian, H., Bergstrøm, B., Ottesen, D., & Rise, L. (2013). Quaternary glaciations and their variations in Norway and on the Norwegian continental shelf. *Quaternary Geology of Norway*, *13*, 27–78.

Ottesen, D., Batchelor, C. L., Dowdeswell, J. A., & Løseth, H. (2018). Morphology and pattern of Quaternary sedimentation in the North Sea Basin (52–62° N). *Marine and Petroleum Geology*, *98*, 836–859. https://doi.org/10.1016/j.marpetgeo.2018.08.022

Ottesen, D., Dowdeswell, J. A., & Bugge, T. (2014). Morphology, sedimentary infill and depositional environments of the Early Quaternary North Sea Basin (56–62° N). *Marine and Petroleum Geology*, *56*, 123–146. https://doi.org/10.1016/j.marpetgeo.2014.04.007

Ottesen, D., Dowdeswell, J. A., Rise, L., & Bugge, T. (2012). Large-scale development of the mid-Norwegian shelf over the last three million years and potential for hydrocarbon reservoirs in glacial sediments. *Geological Society, London, Special Publications*, *368*, 53–73. https://doi.org/10.1144/SP368.6

Ottesen, D., Stewart, M., Brönner, M., & Batchelor, C. L. (2020). Tunnel valleys of the central and northern North Sea (56° N to 62° N): Distribution and characteristics. *Marine Geology*, *425*, 106199. https://doi.org/10.1016/j.margeo.2020.106199

Øygarden, B., Løseth, H., & Njerve, S. (2015). Rock properties of smectite-and ooze-rich claystones. *Geophysics*, *80*, D89–D98. https://doi.org/10.1190/geo2013-0363.1

Platt, N. H., & Cartwright, J. A. (1998). Structure of the east Shetland platform, northern North Sea. *Petroleum Geoscience*, *4*, 353–362. https://doi.org/10.1144/petgeo.4.4.353

Posamentier, H. W. (2004). Seismic geomorphology: Imaging elements of depositional systems from shelf to deep basin using 3D seismic data: Implications for exploration and development. *Geological Society, London, Memoirs*, *29*, 11–24. https://doi.org/10.1144/GSL.MEM.2004.029.01.02

Ringrose, P. S., & Meckel, T. A. (2019). Maturing global CO_2 storage resources on offshore continental margins to achieve 2DS emissions reductions. *Scientific Reports*, *9*, 1–10. https://doi.org/10.1038/s41598-019-54363-z

Rundberg, Y., & Eidvin, T. (2005). Controls on depositional history and architecture of the Oligocene-Miocene succession, northern North Sea Basin. *Norwegian Petroleum Society Special Publications*, *12*, 207–239.

Rundberg, Y., & Eidvin, T. (2016). Discussion on 'Late Cenozoic geological evolution of the northern North Sea: Development of a Miocene unconformity reshaped by large-scale Pleistocene sand intrusion', Journal of the Geological Society, 170, 133–145. *Journal of the Geological Society*, *173*, 384–393.

Singh, V. P., Cavanagh, A., Hansen, H., Nazarian, B., Iding, M., & Ringrose, P. S. (2010). Reservoir modeling of CO_2 plume behavior calibrated against monitoring data from Sleipner, Norway. In *SPE annual technical conference and exhibition*.

Stewart, M. A., Lonergan, L., & Hampson, G. (2013). 3D seismic analysis of buried tunnel valleys in the central North Sea: Morphology, cross-cutting generations and glacial history. *Quaternary Science Reviews*, *72*, 1–17. https://doi.org/10.1016/j.quascirev.2013.03.016

Stocker, T. F. (Ed.) (2014). *Climate change 2013 - the physical science basis. Working Group I contribution to the Fifth assessment report of the Intergovernmental Panel on Climate Change*. Cambridge University Press.

Thibeau, S., & Mucha, V. (2011). Have we overestimated saline aquifer CO_2 storage capacities? In *Oil & Gas Science and Technology – Rev. IFP Energies nouvelles* (Vol. *66*, pp. 81–92).

Thibeau, S., Seldon, L., Masserano, F., Canal Vila, J., & Ringrose, P. (2018). Revisiting the Utsira saline aquifer CO_2 storage resources using the SRMS Classification Framework. In *14th Greenhouse Gas Control Technologies Conference Melbourne* (Vol. *1*, pp. 21–26).

Verdon, J. P., Kendall, J. M., Stork, A. L., Chadwick, R. A., White, D. J., & Bissell, R. C. (2013). Comparison of geomechanical deformation induced by megatonne-scale CO_2 storage at Sleipner, Weyburn, and In Salah. *Proceedings of the National Academy of Sciences*, *110*, E2762–E2771. https://doi.org/10.1073/pnas.1302156110

White, C. M., Strazisar, B. R., Granite, E. J., Hoffman, J. S., & Pennline, H. W. (2003). Separation and capture of CO_2 from large stationary sources and sequestration in geological formations—Coalbeds and deep saline aquifers. *Journal of the Air & Waste Management Association*, *53*, 645–715.

Wrona, T., Magee, C., Jackson, C. A., Huuse, M., & Taylor, K. G. (2017). Kinematics of polygonal fault systems: Observations from the northern North Sea. *Frontiers in Earth Science*, *5*, 101. https://doi.org/10.3389/feart.2017.00101

Zweigel, P., Arts, R., Lothe, A. E., & Lindeberg, E. B. (2004). Reservoir geology of the Utsira Formation at the first industrial-scale underground CO_2 storage site (Sleipner area, North Sea). *Geological Society, London, Special Publications*, *233*, 165–180.